DOPC/DOPE-dependent Effects on Lipid Nanoparticle Stability, Encapsulation, Cytotoxicity, and Cellular Uptake

A Thesis Presented for the

Bachelor of Science

Degree

The University of Tennessee, Knoxville

Graham Cole Goforth

May 2026

Acknowledgments

Words cannot express my gratitude for Dr. Deidra Mountain's mentorship and guidance throughout my research journey. I also could not have undertaken this journey without Caroline Souleyrette and Connor West, the graduate students who generously provided their knowledge and time to support me.

I am also grateful to the University of Tennessee's Department of Biochemistry & Cellular and Molecular Biology for providing me with the opportunity to explore my research interests and deepen my educational experiences.

Lastly, I would be remiss in not mentioning my friends and family, especially my parents and partner. Their belief in me has kept my spirits and motivation high during this process, even if only for a Bachelor's degree.

Abstract

Restenosis after endovascular angioplasty remains a major limitation of vascular interventions, motivating RNA interference strategies that selectively modulate dysfunctional vascular smooth muscle cell (VSMC) remodeling. This study examines how varying the zwitterionic helper lipid 1,2-dioleoyl-sn-glycero-3-phosphatidylcholine (DOPC) with fusogenic 1,2-dioleoyl-sn-glycero-3-phosphatidylethanolamine (DOPE) in our previously patented siRNA-loaded lipid nanoparticles (LNPs) alters clinically relevant attributes and improves VSMC delivery. LNPs containing fixed molar fractions of cholesterol, DSPE-PEG(2000), and stearylated octaargine (STR-R8) were formulated at DOPC/DOPE ratios of 100/0 to 0/100 by direct ethanol injection at a 100:1 lipid:siRNA mass ratio, characterized over 28 days for hydrodynamic diameter, polydispersity index, and siRNA encapsulation/leakage, and then evaluated in primary human aortic smooth muscle cells for cytotoxicity and cellular uptake. Across all compositions, particles remained $\leq$100 nm in diameter, but increasing DOPE content yielded modestly larger, less homogeneous populations, with $\leq$50 mol% DOPE maintaining near-monodisperse distributions while increasing DOPE above 50 mol% resulted in greater polydispersity. Encapsulation efficiencies exceeded 86% for all formulations and increased with higher DOPE content. Cytotoxicity was negligible across all formulations, remaining comparable to baseline cell death at $\leq$ 2.42%. Cellular uptake increased with higher DOPE incorporation, reaching a statistically significant 3-fold enhancement in the 0/100 formulation. Collectively, these results delineate a compositional window in which intermediate DOPE content preserves colloidal stability while augmenting LNP delivery, thereby supporting continued evaluation of DOPE-enriched R8-PLP LNPs as candidates for anti-restenotic RNAi therapy.

Nomenclature

CDH1 Cadherin-1 siRNA

CPP Cell penetrating peptide

CQA Critical Quality Attributes

DLS Dynamic Light Scattering

DOPC 1,2-dioleoyl-sn-glycero-3-phosphatidylcholine

DOPE 1,2-dioleoyl-sn-glycero-3-phosphatidylethanolamine

EE% Encapsulation Efficiency

GAPDH Glyceraldehyde-3-phosphate dehydrogenase siRNA

HASMC Human Aortic Smooth Muscle Cells

LNP Lipid Nanoparticle

PDI Polydispersity Index

PLP Primary Lipid Platform

Rho-PE 1,2-dipalmitoyl-sn-glycero-3-phosphoethanolamine-N-(lissamine rhodamine B sulfonyl)

RNAi RNA Interference

siRNA Small Interfering RNA

STR-R8 Stearylated Octaarginine CPP

Table of Contents

List of Tables

List of Figures

Chapter 1

Introduction

Peripheral vascular disease remains a major clinical burden and frequently requires endovascular or open vascular intervention to restore blood flow in stenotic or occluded vessels. Although procedures such as angioplasty, stenting, atherectomy, bypass grafting, and other peripheral revascularization strategies can improve perfusion, their long-term efficacy is limited by restenosis, a pathological re-narrowing of the treated vessel following vascular injury [44]. Restenosis arises from a coordinated wound-healing response initiated by endothelial disruption and medial injury, including inflammation, vascular smooth muscle cell activation, extracellular matrix remodeling, and neointimal hyperplasia [40]. As the neointima expands, progressive luminal narrowing can compromise vessel patency and necessitate repeat intervention. A central contributor to peripheral restenosis is the proliferation and migration of vascular smooth muscle cells (VSMCs) from the medial layer of the vessel wall into the intima. Following endothelial disruption, VSMCs transition from a contractile phenotype to a synthetic phenotype characterized by enhanced proliferation, migration, and matrix production. This phenotypic switch drives the formation of neointimal tissue that accumulates within the lumen of the vessel. Although the introduction of drug-eluting stents has reduced restenosis rates compared to bare metal stents, these devices remain imperfect solutions. Drug-eluting stents typically release anti-proliferative compounds such as sirolimus or paclitaxel, which suppress VSMC growth but may also delay endothelial healing and increase the risk of late thrombosis [40]. Consequently, there

remains significant interest in the development of alternative therapeutic strategies capable of selectively modulating molecular pathways involved in pathological vascular remodeling.

1.0.1 RNA Interference as a Therapeutic Modality

One promising strategy for regulating disease-associated gene expression is RNA interference (RNAi), a natural biological mechanism that enables sequence-specific silencing of messenger RNA (mRNA). RNAi is mediated by short double-stranded RNA molecules known as small interfering RNA (siRNA), which are incorporated into the RNA-induced silencing complex (RISC). Once loaded into RISC, the antisense strand of the siRNA guides the complex to complementary mRNA transcripts, resulting in the targeted cleavage and degradation of mRNA. This process effectively prevents the translation of the encoded protein, allowing selective suppression of genes implicated in the disease.

The specificity of RNA interference makes it an attractive therapeutic approach for conditions driven by aberrant gene expression, including vascular disease. In the context of vascular restenosis, siRNA therapeutics could theoretically inhibit genes involved in the proliferation, inflammatory signaling, or production of the extracellular matrix of VSMCs. However, despite its therapeutic potential, the clinical application of siRNA faces several significant challenges. Free siRNA molecules are rapidly degraded by nucleases in biological fluids, exhibit poor cellular uptake due to their negative charge and hydrophilicity, and are quickly cleared from circulation. As a result, effective delivery systems are required to protect siRNA molecules and facilitate their transport into target cells.

1.0.2 Lipid Nanoparticles as Delivery Vehicles for RNA Therapeutics

Lipid Nanoparticles (LNPs) have emerged as one of the most effective platforms for the delivery of nucleic acid therapeutics, including siRNA and mRNA. LNP-based delivery systems encapsulate RNA cargo within lipid bilayers or lipid-based structures that protect nucleic acids from enzymatic degradation and enhance cellular uptake. The clinical viability of LNP technology has been demonstrated by several approved therapies, including patisiran,

the first FDA-approved siRNA therapeutic, as well as the mRNA vaccines developed for COVID-19 [1].

LNP formulations typically consist of four primary lipid components: an ionizable or cationic lipid, cholesterol, a polyethylene glycol (PEG) conjugated lipid, and a helper phospholipid. Each component plays a distinct role in determining the nanoparticle structure and function. Ionizable lipids facilitate electrostatic complexation with negatively charged RNA molecules during nanoparticle formation and contribute to endosomal escape after cellular uptake. Cholesterol improves the rigidity and structural stability of the membrane, helping to maintain the integrity of the particles in biological environments. PEGylated lipids provide steric stabilization, reducing particle aggregation, and prolonging circulation time by minimizing interactions with serum proteins. Together, these components form a nanoparticle architecture capable of efficiently delivering nucleic acid cargo to target cells.

1.0.3 Structural Role of Helper Phospholipids in Lipid Nanoparticles

Among the components of LNP formulations, helper phospholipids play a particularly important role in modulating nanoparticle stability, membrane curvature, and intracellular delivery. Helper lipids are typically zwitterionic phospholipids that contribute to the structural organization of the nanoparticle membrane. By influencing lipid packing and membrane phase behavior, these molecules can affect key properties such as particle size, homogeneity, and fusion with cellular membranes.

Two commonly used helper phospholipids in lipid nanoparticle systems are dioleoylphosphatidylcholine (DOPC) and dioleoylphosphatidylethanolamine (DOPE). Although these lipids share similar hydrophobic tails, they differ significantly in their headgroup structures and resulting biophysical properties. DOPC contains a phosphatidylcholine headgroup that promotes a cylindrical molecular geometry, favoring the formation of stable lamellar bilayer structures. This property tends to enhance the stability of the nanoparticles and maintain uniform particle distributions.

In contrast, DOPE possesses a smaller phosphatidylethanolamine headgroup that produces a cone-shaped molecular geometry. This geometry promotes the formation of non-lamellar phases, particularly the inverted hexagonal (HII) phase, which is associated with increased membrane curvature and fusogenic behavior. As a result, DOPE-containing membranes exhibit enhanced propensity for membrane fusion and destabilization. In the context of nucleic acid delivery systems, these properties can facilitate endosomal escape by promoting fusion between the nanoparticle membrane and endosomal membranes following cellular uptake.

1.0.4 Influence of Lipid Composition on Nanoparticle Stability and Delivery

The physicochemical properties of lipid nanoparticles are strongly influenced by their lipid composition. Key parameters such as hydrodynamic diameter, polydispersity index (PDI), and encapsulation efficiency are often referred to as critical quality attributes (CQAs) of nanoparticle formulations. These attributes directly impact nanoparticle stability, biodistribution, and therapeutic efficacy.

The polydispersity index provides a measure of particle size heterogeneity within a formulation. Low PDI values indicate uniform nanoparticle populations, whereas higher values suggest broader size distributions and an increased likelihood of aggregation. Similarly, encapsulation efficiency reflects the proportion of nucleic acid successfully packaged within the nanoparticle carrier. High encapsulation efficiency is desirable because it maximizes the effective dose of therapeutic cargo delivered to target cells.

Modifying helper lipid composition can significantly influence these parameters. Incorporation of fusogenic lipids such as DOPE may enhance intracellular delivery by improving membrane fusion and endosomal escape, but this benefit may come at the cost of reduced nanoparticle stability or increased heterogeneity. Conversely, more structurally stable lipids, such as DOPC, may produce more uniform nanoparticles but may limit membrane fusion and intracellular cargo release. Identifying an optimal balance between these competing

factors is therefore a critical step in optimizing nanoparticle formulations for therapeutic applications.

1.0.5 Lipid Nanoparticle Delivery to Vascular Smooth Muscle Cells

Effective treatment of vascular restenosis requires therapeutic agents capable of targeting vascular smooth muscle cells within the arterial wall. VSMCs are key mediators of neointimal hyperplasia, and suppression of their proliferation represents a promising strategy to prevent pathological vessel remodeling. Lipid nanoparticles offer a potential means of delivering siRNA therapeutics directly to these cells, enabling selective silencing of genes that drive pathological vascular responses.

However, successful delivery of nucleic acid therapeutics to VSMCs presents several challenges. Nanoparticles must be sufficiently stable to maintain structural integrity during circulation, but capable of efficiently interacting with cellular membranes to enable uptake and intracellular release of their cargo. The lipid composition is a critical determinant of these properties, influencing both the nanoparticle stability and the efficiency of cellular delivery. Consequently, systematic investigation of how specific lipid components affect nanoparticle behavior is essential for the rational design of optimized delivery systems.

1.0.6 Research Objective

The objective of this project is to evaluate how the substitution of the helper phospholipid DOPE for DOPC within an siRNA lipid nanoparticle formulation influences nanoparticle stability, encapsulation efficiency, cytotoxicity, and cellular uptake in human aortic smooth muscle cells. Lipid nanoparticles were synthesized using a direct ethanol injection method and formulated with varying molar ratios of DOPC and DOPE while maintaining constant proportions of cholesterol, PEGylated lipid, and a cationic peptide lipid component. This experimental design allows a systematic assessment of how helper lipid composition affects key nanoparticle characteristics relevant to therapeutic delivery.

It is hypothesized that an increase in the DOPE content will enhance cellular uptake due to its fusogenic membrane properties but also increases the size and heterogeneity of the nanoparticles due to reduced membrane packing stability. In contrast, formulations enriched in DOPC are expected to exhibit greater structural stability but potentially lower intracellular delivery efficiency. By characterizing how these compositional changes influence critical nanoparticle properties, we aimed to identify a formulation window that balances nanoparticle stability with enhanced functional delivery outcomes.

Chapter 2

Background

2.1 Nanoparticle Platforms in the Biological Sciences

Nanoparticles are typically defined as particulate materials with at least one dimension in the $\simeq$ 1-100 nm range, although in some biomedical practice the term is often used more broadly to encompass "nanoscale" carriers whose transport, surface chemistry, and biological interactions differ qualitatively from bulk materials. At these length scales, a high surface-area-to-volume ratio and curvature-driven packing effects make surface composition (charge, hydrophilicity, and ligand display) a primary determinant of colloidal stability, protein adsorption, and cell/tissue interactions.

In drug delivery, this is exploited to solubilize or protect cargo, which can be small molecules, proteins, or nucleic acids; to control pharmacokinetics via steric stabilization and reduced opsonization; and to enable cell entry and intracellular trafficking. For tumors and some inflamed tissues, nanoparticle accumulation has historically been rationalized by the enhanced permeability and retention effect (EPR), although its magnitude is variable between disease contexts and patients [31].

A central biological principle is that nanoparticles rapidly acquire an adsorbed "protein corona" in physiological fluids, which can re-specify their effective 'identity' by altering targeting, clearance, biodistribution, and immune recognition [39, 5]. Consequently, nanoparticle characterization for biological work must go beyond nominal composition to include size distributions using DLS or NTA; morphology using transmission electron

microscopy (TEM) or cryogenic electron microscopy (cryo-EM); surface charge by zeta potential; stability in relevant media of serums and buffers; and batch-to-batch reproducibility—because these features map directly onto clearance routes, tissue access, and cellular uptake mechanisms. Safety considerations also emerge from nanoscale-specific considerations: adverse outcomes often relate to surface reactivity, immunostimulation or complement activation, oxidative stress, or persistence/accumulation (particularly for some inorganic nanoparticles), motivating early evaluation of cytotoxicity, inflammatory signaling, hemocompatibility, and organ biodistribution.

2.1.1 Polymeric Nanoparticles

Polymeric nanoparticles are engineered colloids, typically ranging between ten and a few hundred nanometers, that use tunable polymer chemistry to solubilize and protect labile payloads; to modulate pharmacokinetics and biodistribution by controlling size, surface charge, and corona formation; and to program release kinetics via diffusion, swelling, and/or polymer degradation. In practice, biodegradable polyesters, such as poly[lactic-co-glycolic acid] (PLGA) and related copolymers, hydrophilic shells incorporating PEGylation, and stimulus-responsive motifs are selected to address dominant *in vivo* barriers—protein adsorption and clearance, extravasation/penetration into diseased tissue, cellular uptake, and intracellular trafficking—thereby improving the therapeutic index relative to free drug. This design logic is central to contemporary paradigms of "precision nanoparticle" development that treat nanoparticle physicochemical properties as adjustable parameters for adjusting heterogeneous biological barriers between diseases and populations of patients.

The most mature applications are in drug delivery, especially in oncology and chronic inflammatory disease, where polymeric nanoparticles enable sustained exposure while reducing off-target toxicity and enabling passive and active targeting strategies.

2.1.2 Inorganic Nanoparticles

Inorganic nanoparticles (INPs) are nanoscale carriers, typically 1 to 100 nm in size, whose core is composed of inorganic matter which is most commonly metals (e.g. silver, gold),

metal oxides (e.g. iron oxides), silica-based formulations or semiconductor nanocrystals (quantum dots). Biological performance is determined by both the surface chemistry and properties of the core materials, as well. In applications, INPs are most often engineered as core-shell and/or coated colloids that include an inorganic core that confers some form of physical function, such as plasmonic absorption, magnetism, fluorescence, or X-ray attenuation; a stabilizing shell or coating, sometimes made of silica, polymers, PEG, or zwitterionic ligands that control dispersion and nonspecific interactions; and optional functional ligands or payloads that are coupled to or loaded within the particle [16]. This modular architecture is central to why INPs are prominent in biological sciences: they provide tunable physicochemical properties that enable molecular imaging, biosensing, and stimuli-responsive therapy, and can be integrated into multifunctional "theranostic" constructs [24].

Representative INP platforms illustrate the structure-function logic that underlies their biological relevance. Gold nanoparticles exploit localized surface plasmon resonance to support sensitive optical detection and light-to-heat conversion for photothermal intervention [22]. Mesoporous silica nanoparticles provide high surface area and tunable pore networks that enable high-capacity loading and stimuli-responsive release of therapeutic cargos [42]. Quantum dots offer exceptional brightness and photostability for labeling and ultrasensitive detection, while their use in vivo depends critically on surface passivation and bioconjugation to manage stability and biocompatibility [6]. Together, these examples underscore the unifying theme that INPs are best understood as engineered multicomponent systems in which the inorganic core supplies a physical modality and the surface interface governs biological performance.

2.1.3 Viral-Mimetic and Hybrid Nanoparticles

Viral-mimetic and hybrid nanoparticle systems are best understood as design strategies rather than entirely separate nanoparticle classes. In nucleic acid delivery, a formulation may be considered viral-mimetic when it incorporates functional features that resemble viral delivery mechanisms, such as efficient membrane binding, cellular internalization, endosomal escape, or membrane fusion. Similarly, hybrid nanoparticles combine synthetic carrier architectures with biologically inspired or functional components, including fusogenic lipids,

cell-penetrating peptides (CPPs), targeting ligands, polymer-lipid domains, or membrane-derived materials. In this sense, lipid nanoparticles can themselves be engineered as viral-mimetic or hybrid systems when their lipid composition or surface functionality is designed to reproduce selected viral-like delivery behaviors.

A central feature of viral-mimetic design is the incorporation of fusogenic lipid components that promote membrane destabilization under endosomal conditions. Phosphatidylethanolamine-containing lipids, such as DOPE, exhibit a cone-shaped molecular geometry that favors formation of non-lamellar phases, including the inverted hexagonal phase, which is associated with membrane fusion and disruption. This behavior has been extensively linked to improved endosomal escape and intracellular delivery efficacy in lipid-based systems [36]. Within LNP formulations, such helper lipid effects are particularly important, as the behavior of the membrane phase directly influences the ability of NPs to release encapsulated nucleic acids into the cytosol.

Hybrid nanoparticle systems further expand this paradigm by combining synthetic lipid architectures with biologically inspired or functionalized components, including cell-penetrating peptides, targeting ligands, or polymer-lipid composites. These additions enable multivalent interactions with cellular membranes and can enhance uptake through receptor-mediated pathways. For example, arginine-rich peptides have been shown to increase cellular internalization through electrostatic interactions with negatively charged cell surfaces, a mechanism analogous to viral adsorption. Such strategies are directly relevant to peptide-functionalized LNP systems, where surface modification is used to enhance delivery efficiency without fundamentally altering the nanoparticle core composition.

Despite these advantages, viral-mimetic systems introduce additional formulation complexity. Integration of multiple functional components can have an impact on particle stability, biodistribution, and immunogenicity, often in nonlinear ways. Consequently, while viral-mimetic and hybrid nanoparticles can significantly improve delivery efficiency, they require careful optimization to maintain reproducibility and translational feasibility.

2.1.4 Extracellular Vesicles and Biomimetic Nanoparticles

Extracellular vesicles (EVs) and biomimetic nanoparticles represent a biologically derived or biologically inspired class of delivery systems that leverage endogenous membrane structures to enhance compatibility with physiological environments. EVs, including exosomes and microvesicles, are naturally secreted lipid bilayer vesicles that mediate intercellular communication and transport biomolecules such as RNA, proteins, and lipids. Their intrinsic biological origin provides several advantages for therapeutic delivery, including stability in circulation, reduced immunogenicity, and efficient cellular uptake.

A defining characteristic of EV-based systems is their native membrane composition, which includes complex lipid mixtures and membrane-associated proteins that facilitate interaction with recipient cells. These features enable EVs to undergo efficient endocytosis and, in some cases, direct membrane fusion, thus promoting intracellular cargo delivery. As a result, EVs have been widely investigated as carriers for RNA therapeutics, where they can protect nucleic acids from degradation while maintaining delivery efficiency [33].

Biomimetic nanoparticle systems extend this concept by combining EV-derived or cell membrane components with synthetic nanomaterials. One prominent example is the development of cell membrane-coated nanoparticles, in which synthetic cores are cloaked with natural membrane material to confer immune evasion and prolonged circulation time [25]. Similarly, hybrid EV-liposome systems have been engineered to improve cargo loading capacity while preserving the biological functionality of native vesicles.

However, EV-based systems face significant translational challenges. Isolation and purification techniques often yield heterogeneous populations, and large-scale production remains difficult compared to established nanoparticle manufacturing methods. Additionally, cargo loading efficiency is less controllable than in engineered LNP systems, limiting their reproducibility in therapeutic contexts. Consequently, while EVs and biomimetic nanoparticles offer clear advantages in terms of biocompatibility and targeting, they are currently best positioned as complementary or hybrid platforms rather than direct replacements for fully synthetic LNP systems.

2.1.5 Lipid Nanoparticles

A defining characteristic of LNP behavior in vivo is that exposure to biological fluids leads to rapid adsorption of proteins and other biomolecules, forming a biomolecular (protein) corona that often becomes the effective "biological identity" of the particle, shaping cellular recognition, uptake pathways, biodistribution, and toxicity [32]. Consequently, the canonical design variables—hydrodynamic size, surface charge (zeta potential), ligand density, and colloidal stability—are not only formulation details but determinants of biological fate; systematic work has shown that nanoparticle size and surface properties strongly influence the composition and persistence of the corona and thus downstream biointeractions [30]. This explains why the same lipid nanoparticle can exhibit markedly different biological outcomes depending on the coating chemistry and dispersion state, and why rigorous characterization in relevant media is essential for translational interpretation.

2.2 RNA Interference (RNAi)

2.2.1 Definition and Mechanism

RNA interference (RNAi) is a conserved, sequence-directed gene regulatory process in which double-stranded RNA (dsRNA) or structured RNA precursors are converted into small guide RNAs that program ribonucleoprotein effector complexes to repress complementary nucleic acid targets. Functionally, RNAi acts as a post-transcriptional gene-silencing system in many eukaryotes, with additional roles in transcriptional silencing and chromatin regulation in various organisms and other contexts. The modern definition of RNAi emerged from the demonstration that introducing dsRNA into *Caenorhabditis elegans* elicits potent and highly specific suppression of cognate gene expression [12], and from subsequent biochemical evidence that dsRNA triggers a programmable nuclease pathway in animal cells [20]. Collectively, these findings established RNAi as an information-processing pathway: sequence information carried by small RNAs is translated into selective repression of matching transcripts.

Initiation: dsRNA processing by RNase III Enzymes (Dicer family)

A central biochemical step is the conversion of long dsRNA into short duplex products by an endonuclease of the RNase III-family, Dicer. Genetic and mechanistic studies in animals linked Dicer to the production of small RNA species that accumulate during silencing and are required for downstream target recognition sources. Dicer cleavage yields small RNA duplexes bearing 5' phosphates and 2-nucleotide 3' overhangs—structural signatures consistent with RNase III processing and critical for downstream sorting and loading. The concept that defined-length short duplexes are sufficient to trigger sequence-specific silencing in mammalian cells, rather than long dsRNA that can activate innate immune responses, was demonstrated by showing that synthetic 21-nucleotide duplexes can induce robust and specific repression in cultured mammalian cells [10]. This observation is important because it separates the processing requirement (Dicer-mediated generation of guides) from the effector requirement (RISC-mediated repression). Thus, if a cell is provided with appropriately structured short duplexes, it can bypass upstream dsRNA processing and directly engage the effector machinery.

RISC assembly: guide selection and Argonaute loading

Following Dicer-mediated production or exogenous supply of the small RNA duplex, the duplex is transferred into a loading pathway that culminates in the association of Argonaute. During RISC maturation, one strand is retained as a guide, while the other "passenger" strand is removed, resulting in an active complex capable of binding to the target. The biochemical identification of a programmable nuclease complex in *Drosophila* cell extracts provided early evidence for an RNA-guided effector entity consistent with RISC [20]. Subsequent work established the Argonaute proteins as the catalytic and structural core of RISC, including direct evidence that mammalian Argonaute2 (Ago2) provides "slicer" endonuclease activity responsible for guide-directed cleavage of target RNAs when complementarity is sufficient [41]. In practical terms, this implies that the *degree* and *geometry* of guide-target pairing govern the repression mode. Near-perfect pairing, common in many siRNA contexts, favors endonucleolytic cleavage, while partial pairing, typical of

many endogenous small RNA interactions, more often results in translational repression or deadenylation-dependent decay.

Target recognition and repression outputs

Once mature, RISC surveys cellular transcripts by Watson-Crick base pairing between the guide strand and candidate targets. After binding, repression can proceed through direct endonucleolytic cleavage of target RNA (Ago2-mediated slicing in mammals when pairing is extensive), recruitment of decay machinery that accelerates deadenylation and turnover, and/or inhibition of translation [43]. Although these outcomes are frequently discussed in the context of specific small RNA classes, such as siRNA versus miRNA, the unifying mechanistic principle at the RNAi level is that small RNAs provide sequence specificity, while Argonaute-centered effector complexes provide the biochemical "actuator" functions that reduce gene output.

Amplification, spreading, and system-level behavior

A further mechanistic layer, prominent in plants and some animals, is signal amplification and systemic spread. In these systems, RNA-dependent RNA polymerases (RdRPs) can use targeted transcripts as templates to generate additional dsRNA, thereby amplifying silencing and enabling propagation beyond the initially targeted cell. This feature explains why RNAi can behave as a robust antiviral and transposon-control strategy at the organismal scale, whereas in many mammalian somatic contexts RNAi is typically modeled primarily as an intracellular, non-amplifying silencing process. Comprehensive reviews synthesize these organismal differences and provide a standardized framework for mapping "initiation $--> $ RISC loading $--> $ repression" while noting where amplification and nuclear silencing modules are operative.

Relevance to various RNA Modalities

This mechanistic scaffold is the conceptual prerequisite for understanding why different nucleic-acid modalities behave differently. siRNA and shRNA largely exploit the RNAi machinery by supplying duplex guides or duplex-generating precursors that feed into

Dicer/Argonaute pathways. miRNAs represent endogenous regulatory guides that are processed and loaded by related principles but often act through partial complementarity. Antisense oligonucleotides (ASOs) frequently engage distinct effector proteins, such as RNase H, rather than canonical RISC, despite superficial similarities in "sequence-directed repression" [2].

2.2.2 Major RNA Modalities

Short Hairpin RNA (shRNA)

Short Hairpin RNA (shRNA) is an engineered, single-stranded RNA transcript that folds into a defined stem-loop (hairpin) structure and functions as a vector-expressed trigger of RNA interference. In mammalian systems, shRNA are commonly transcribed from RNA polymerase III promoters (e.g., U6 or H1), yielding short hairpin precursors that are exported from the nucleus and subsequently processed into 21-nucleotide siRNA-like duplexes by the endogenous RNAi machinery [45, 35]. The resulting guide strand is incorporated into RISC and follows a pathway comparable to siRNA's mechanism of action.

A principal advantage of shRNA over exogenously delivered siRNA is the potential for sustained knockdown, because the hairpin is continuously transcribed in transduced or stably selected cells, supporting longer-duration phenotypic studies and pooled loss-of-function screens. However, because shRNAs intersect with endogenous small-RNA biogenesis and trafficking pathways, knockdown efficacy and safety are strongly expression-level dependent. Excessive shRNA production can saturate limiting host factors, including export and processing components shared with microRNA pathways, leading to dysregulation of endogenous microRNAs, and in vivo, dose-dependent toxicity [8]. Consequently, robust shRNA applications typically emphasize careful hairpin design, promoter selection, and/or regulated expression, and empirical titration of vector dose to balance potency with pathway load.

MicroRNA (miRNA)

MicroRNAs (miRNAs) are endogenous, 21-23 nucleotide non-coding RNAs that post-transcriptionally regulate gene expression by guiding Argonaute-containing silencing complexes to complementary sites in target transcripts. miRNAs were first recognized through genetic studies of developmental timing in *C. elegans* for lin-4 and let-7, which established that small RNAs can act as sequence-specific regulators by base pairing with messenger RNAs [37, 26]. Subsequent work demonstrated that miRNAs are widespread across animals and plants and constitute a major layer of gene regulation, with individual miRNAs often influencing suites of functionally related targets [3].

Canonical miRNA biogenesis begins with transcription of miRNA genes, commonly by RNA polymerase II, producing long primary transcripts (pri-miRNAs) that can be capped and polyadenylated [28]. In the nucleus, the microprocessor complex—Drosha with DGCR8—cleaves pri-miRNAs to yield approximately 60 to 70 nucleotide hairpin precursors (pre-miRNAs) [21, 27]. Pre-miRNAs are then exported to the cytoplasm in an Exportin-5/Ran-GTP-dependent manner and further processed by Dicer to generate an approximately 22 nucleotide miRNA duplex, from which a mature guide strand is loaded into Argonaute to form the core effector complex.

Functionally, miRNAs recognize targets primarily through partial complementarity, with "seed" pairing (often nucleotides 2-7/8) acting as a dominant specificity determinant in many animal systems [4, 7]. Target enhancement can repress protein output via translational inhibition, and, frequently, by accelerating mRNA deadenylation or decay. In mammalian cells, reductions in target mRNA abundance account for most measurable repression for many miRNA-target interactions [18]. Through these interactions, miRNAs help buffer transcriptional noise and coordinate developmental programs, differentiation, proliferation, and stress responses, and their dysregulation is widely implicated in human disease [4].

Antisense Oligonucleotides (ASOs)

Antisense oligonucleotides (ASOs) are short, synthetic, single-stranded nucleic acids designed to bind complementary RNA sequences through Watson-Crick base pairing,

thereby modulating gene expression at the RNA level [38]. In therapeutic contexts, ASOs operate primarily via two mechanistic classes. "RNase H1-active" ASOs form DNA-like heteroduplexes with target RNA, recruiting RNase H1 to cleave the RNA strand and reduce transcript abundance, whereas "steric-blocking" ASOs (often termed splice-switching oligonucleotides) bind pre-mRNA or mRNA to occlude regulatory motifs, such as splice silencers, enhancers, or translation elements, without nuclease recruitment to alter isoform usage or RNA processing [29, 9]. This conceptual flexibility enables ASOs to address both gain- and loss-of-function pathobiology by either decreasing toxic RNA/protein output or restoring productive RNA processing.

Clinical viability of ASOs has depended on iterative chemical optimization to improve nuclease resistance, target affinity, and pharmacokinetics while controlling toxicity [15]. The most widely deployed platform integrates a phosphorothioate (PS) backbone to increase stability and plasma protein binding, paired with 2'-ribose modifications such as 2'-O-(2-methoxyethyl), 2'-O-methyl, or 2'-fluoro, that enhance hybridization affinity and durability in tissue [15, 11]. "Gapmer" architectures—modified "wings" flanking a central DNA "gap"—are specifically engineered to retain RNase H competence while exploiting high-affinity chemistries at the termini. Biodistribution after systemic dosing is generally broad but biased toward liver and kidney, with cellular uptake dominated by endocytosis and endosomal trafficking representing a key potency bottleneck [11, 38]. Accordingly, modern delivery strategies frequently employ ligand conjugation, most notably GalNAc for hepatocyte targeting, or local administration routes, such as intrathecal dosing for central nervous system exposure [29, 15].

The clinical maturation of ASOs is exemplified by Nusinersen, which corrects SMN2 splicing to increase full-length SMN protein in spinal muscular atrophy, producing clinically meaningful improvements in infantile-onset disease when administered intrathecally [46]. Beyond standardized drugs, the platform has also enabled rapid, patient-customized oligonucleotide development for ultra-rare genetic disorders, underscoring the modularity of sequence-defined therapeutics. Nevertheless, ASO development requires careful management of sequence-dependent and chemistry-dependent risks, including hybridization-mediated off-target effects, as well as class-associated tolerability liabilities that can involve immune

activation and organ-specific toxicities [**?** 46]. Ongoing advances in backbone stereochemistry, high-affinity sugar chemistries, and targeted delivery are therefore central to expanding therapeutic windows and broadening tissue reach [29, 15].

Small Interfering RNA (siRNA)

Small interfering RNA (siRNA) refers to short, double-stranded RNA duplexes that are most often 21 to 23 nucleotides in length, for functional applications [34]. siRNAs mediate sequence-specific, post-transcriptional gene silencing through the RNA interference (RNAi) pathway. Following cytosolic entry, one strand of the duplex (termed the "guide" strand) is preferentially loaded into the Argonaute-containing RNA-induced silencing complex (RISC), while the complementary strand is discarded [41]. The guide strand directs RISC to complementary messenger RNA (mRNA) transcripts via Watson-Crick base pairing. When complementarity is high, Argonaute-2 can catalyze endonucleolytic cleavage of the target mRNA, which is subsequently degraded, resulting in reduced translation and diminished protein expression. Given siRNA activity is governed by nucleotide-level complementarity, it enables highly programmable knockdown of genes implicated in disease-relevant cellular phenotypes.

In biomedical research and therapeutics, siRNA has become a foundational modality for transient gene suppression and target validation, and it has progressed into clinical use for select indications. However, effective siRNA application is constrained by pharmacologic and biologic barriers, including rapid nuclease degradation, unfavorable biodistribution, limited membrane permeability, and inefficient endosomal escape. As a result, siRNA is commonly paired with chemical modifications to enhance stability and reduce innate immune recognition as well as delivery systems to improve circulation time, tissue uptake, and cytosolic release.

2.3 Phospholipids in Lipid Nanoparticles

2.3.1 DSPC (1,2-distearoyl-sn-glycero-3-phosphocholine)

1,2-distearoyl-sn-glycero-3-phosphocholine (DSPC) is a zwitterionic phosphatidylcholine (PC) characterized by a bulky choline headgroup and two fully saturated C18:0 (stearoyl) acyl chains. This combination yields an approximately cylindrical molecular geometry that preferentially supports lamellar (bilayer) organization and tight lipid packing. In LNP formulations, DSPC is commonly employed as a "helper" phospholipid to stabilize the supramolecular structure by promoting ordered membrane domains and increasing resistance to deformation. Consistent with its saturated tails and associated high gel-liquid crystalline transition temperature (T_m), DSPC is strongly linked to enhanced mechanical robustness and colloidal stability of the particle over storage and circulation-relevant conditions [19].

DSPC has a prominent design legacy in clinically deployed nucleic acid LNPs, in part because it inherits manufacturability and stability advantages from earlier liposomal drug products. However, the same ordered, tightly packed bilayer propensity that improves structural stability can reduce membrane fusogenicity and thereby disfavor endosomal membrane fusion events unless it is compensated by other formulation elements that drive endosomal disruption. Comparative studies in vitro indicate that PC-containing systems, relative to PE-containing analogs, may exhibit higher endocytosis and cellular uptake readouts, while downstream functional cytosolic delivery remains dependent on the full lipid composition and intracellular processing steps [23].

2.3.2 DOPC (1,2-dioleoyl-sn-glycero-3-phosphocholine)

1,2-Dioleoyl-sn-glycero-3-phosphocholine (DOPC) is a zwitterionic PC with the same choline headgroup class as DSPC, but it contains two monounsaturated C18:1 (oleoyl) chains. The cis double bonds introduce conformational "kinks" in the hydrophobic tail, reducing packing efficiency and shifting the membrane toward higher fluidity and lower order than saturated PC analogs. As a helper phospholipid within nanoparticles, DOPC biases the lipid matrix toward a more dynamic, less densely packed interfacial environment, which

can influence particle morphology, lipid exchange kinetics, and interactions within biological membranes during cellular uptake and intracellular trafficking [19].

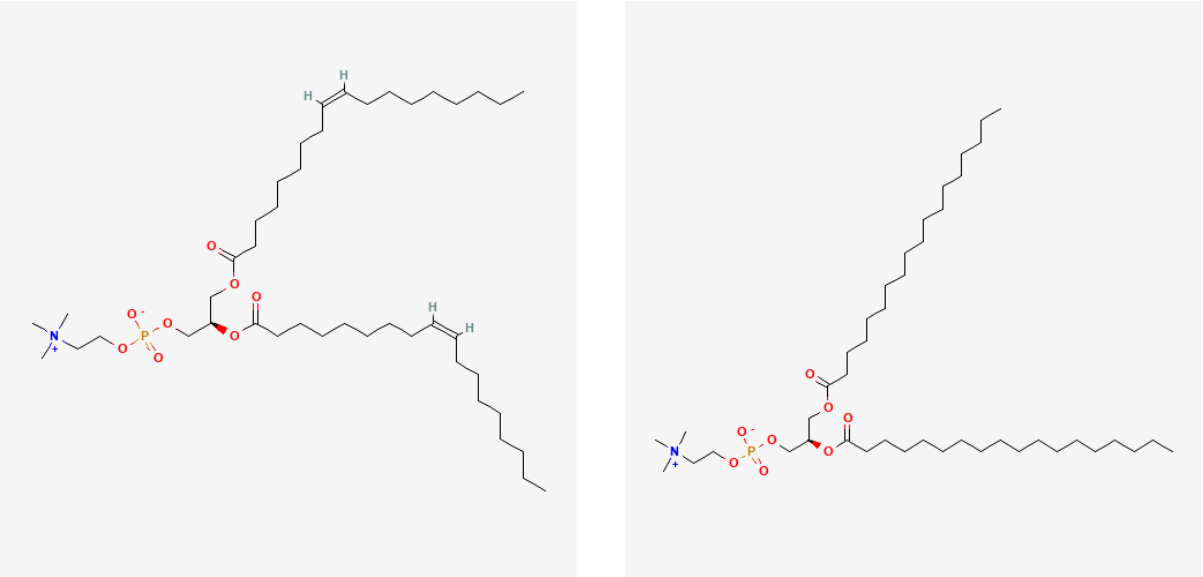

(a) DOPC **(b)** DSPC

Figure 2.1: Structure of Helper Phospholipids DOPC vs DSPC

Functionally, replacing saturated PC components (e.g. DSPC) with unsaturated PC species (e.g. DOPC) has been associated, in specific in vitro delivery models, with increased cellular uptake and increased intracellular delivery metrics, emphasizing that helper-lipid acyl-chain unsaturation can meaningfully impact particle-cell interactions [17]. Importantly, these effects are context-dependent, such as the serum/protein environment, and should be interpreted as formulation- and model-dependent rather than intrinsic guarantees of improved delivery for all LNP systems.

2.3.3 DOPE (1,2-dioleoyl-sn-glycero-3-phosphoethanolamine)

1,2-Dioleoyl-sn-glycero-3-phosphoethanolamine (DOPE) is a zwitterionic phosphatidylethanolamine (PE) distinguished by a smaller headgroup than PC lipids and two monounsaturated C18:1 (oleoyl) chains [fig. 2.2a]. This architecture produces a truncated-cone molecular shape, with small headgroup relative to its bulky hydrophobic volume, that favors negative membrane curvature and non-lamellar phase behavior [19]. In LNP design, DOPE is classically

described as a fusogenic helper lipid that preferentially stabilizes inverted hexagonal and related non-bilayer structures that are mechanistically linked to bilayer destabilization, membrane fusion, and disruption processes relevant to endosomal escape.

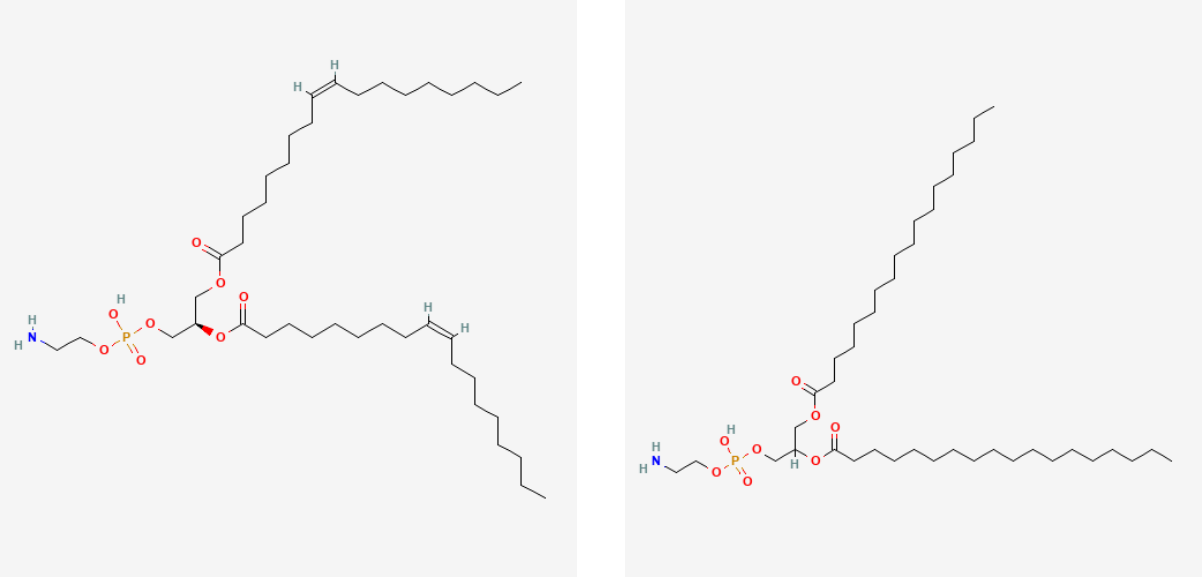

(a) DOPE **(b)** DSPE

Figure 2.2: Structure of Helper Phospholipids DOPE vs DSPE

In practical formulation terms, incorporating DOPE can shift the helper-lipid contribution away from purely stabilizing lamellar order and toward curvature-driven membrane remodeling, complementing ionizable or cationic components that become protonated during endosomal maturation and participate in disruption/fusion phenomena [23]. Moreover, literature summarized in LNP reviews note that DOPE-containing formulations have, in some mRNA delivery platforms, produced higher expression outcomes than DSPC-containing counterparts, reinforcing the role of PE-driven non-lamellar propensity as a mechanism for enhancing intracellular delivery steps that occur after cellular uptake.

2.4 Patented R8-PLP Formulation

2.4.1 Platform Composition and Attributes

The Vascular Research Laboratory at the University of Tennessee Medical Center has developed a patented "PLP/R8-PLP" system that is a neutral, PEGylated lipid nanoparticle (PLP) chassis that is functionalized with an amphiphilic octaarginine (R8) derivative to improve nucleic acid loading and cell association without converting the bulk carrier into a strongly cationic lipid formulation. In the representative PLP formulation described within the patent family, bulk membrane lipid is DOPC:cholesterol at 7:3 (mol:mol) with 10 mol% DSPE-PEG(2000) as the steric stabilizer defining the PEGylated, colloidally stable baseline carrier [14, 13]. The platform formulation introduces R8 as either stearylated R8 (STR-R8), a membrane-anchored cell-penetrating peptide (CPP) and condenser, or PEG-R8 (R8 presented via a PEG-lipid conjugate) with STR-R8 specifically evaluated across 0-10 mol% and an empirically selected operating point at 10 mol% STR-R8 for subsequent experiments.

A central technical claim across these disclosures is that high siRNA loading can be achieved in an otherwise noncationic bilayer by pairing ethanol-injection liposome formulation with divalent-cation-mediated condensation using $CaCl_2$ and STR-R8 as a lipid-anchored "nucleic acid condenser" that can also function as a CPP. Within the optimization examples, Ca^{2+} is tested from 0-50 mM with $\approx$ 10 mM Ca^{2+} identified as the lowest concentration producing a marked increase in encapsulation efficiency in both PLP and R8-PLP contexts. In a specific example, 10 mol% STR-R8 increased encapsulation relative to PEGylated PLP alone, and adding 10 mM Ca^{2+} further increased encapsulation versus STR-R8 without calcium. The patents additionally report process-parameter dependence (e.g. lipid:siRNA weight ratio testing, injection-rate effects) as controllable factors for loading and homogeneity, with an explicit example of 100:1 lipid:siRNA (wt:wt) yielding very high encapsulation in the stated system [14, 13].

With respect to the platform's quality attributes, the patent and applications emphasize that the condenser-enabled loading strategy is compatible with maintaining sub-100 nm nanoparticles, and in the worked examples the STR-R8/ Ca^{2+} condition is reported to preserve particle size in the $\approx$ 50-60 nm range while keeping polydispersity low at 0.2

under certain injection conditions [14]. For cellular compatibility and interaction, the patents operationalize performance in smooth muscle-relevant models by quantifying cellular uptake after dosing with 50 μM total lipid using rhodamine-labeled liposomes, aligning the platform's functional intent with CPP-enabled association and uptake while preserving an architecture that remains predominantly neutral/PEG-stabilized.

2.4.2 Experimental Justification

These disclosures also preserve substantial experimental latitude for the present thesis, because this patented PLP is defined primarily as a neutral, PEG-stabilized phospholipid/sterol chassis that is then modularly augmented with STR-R8 and divalent cations to satisfy nucleic acid loading and cell interaction requirements. Systematically varying the DOPC/DOPE ratio, therefore, constitutes a direct, hypothesis-driven exploration within the patented design space. By holding constant the platform-defining elements–PEG-lipid fraction, sterol content, and STR-R8 incorporation/assembly strategy— while turning the DOPC:DOPE balance, this work can resolve how helper-lipid composition governs tradeoffs among long-term colloidal stability (size and PDI drift), siRNA cargo retention, and cellular compatibility.

Chapter 3

Materials and Methods

3.1 Lipid Nanoparticle Assembly

3.1.1 Lipid Nanoparticle Formulation Constituents

All lipids and cholesterol were obtained from Avanti Polar Lipids, Inc. (Alabaster, AL, USA). Stearylated octaarginine (STR-R8) was purchased from LifeTein LLC (Somerset, NJ, USA).

Table 3.1: Lipid Formulation Constituents

Acronym	Lipid Constituent
Chol.	Cholesterol
DOPC	1,2-dioleoyl-sn-glycero-3-phosphatidylcholine
DOPE	1,2-dioleoyl-sn-glycero-3-phosphatidylethanolamine
DSPE-PEG	1,2-distearoyl-sn-glycero-3-phosphoethanolamine-N -[methoxy(polyethylene glycol)-2000]
STR-R8	Stearylated octaarginine

3.1.2 Synthesis of Lipid Nanoparticles

Base R8-PLP lipid nanoparticles (LNPs) were formulated with cholesterol, DSPE-PEG(2000), and STR-R8 at fixed molar fractions of 24 mol%, 10 mol%, and 10 mol%, respectively. The remaining 56 mol% of the lipid composition was apportioned between the DOPC and DOPE to yield the experimental DOPC/DOPE molar ratios of 100/0, 75/25,

50/50, 25/75, and 0/100. Across all formulations, the total nanoparticle mass was held constant at 1.00 mg.

All LNPs were prepared by direct ethanol injection at a lipid:siRNA mass ratio of 100:1 (w/w). Individual lipid components were dissolved in chloroform ($CHCl_3$), combined according to the designated formulation (see Appendix A), and dried under a stream of nitrogen gas to remove residual solvent. The dried lipid film was reconstituted in molecular-grade absolute ethanol (EtOH), incubated for 1 hr at 37 °C, then added dropwise to an aqueous phase consisting of 10 mM Tris-HCl (pH 8.0) supplemented with 10 mM $CaCl_2$ and 750 pmol siRNA. Either GAPDH-targeting siRNA (functional) or CDH1 siRNA (nonfunctional negative control) was used (ThermoFisher Scientific, Waltham, MA, USA). Injections were performed at an EtOH:aqueous volume ratio of 2:3 under continuous vortex mixing at room temperature. Formulations were dialyzed for 24 h against phosphate-buffered saline (PBS; pH 7.4) at 4 °C to remove ethanol, and subsequently extruded through a 100 nm polycarbonate membrane using a TWIST mini-extruder prior to downstream analysis (Helix Biotech, Knoxville, TN, USA).

Table 3.2: Control and Experimental R8-PLP Formulation Components

	Chol.	**DOPC**	**DOPE**	**DSPE-PEG**	**STR-R8**
100/0	24 mol%	56 mol%	0 mol%	10 mol%	10 mol%
75/25	24 mol%	42 mol%	14 mol%	10 mol%	10 mol%
50/50	24 mol%	28 mol%	28 mol%	10 mol%	10 mol%
25/75	24 mol%	14 mol%	42 mol%	10 mol%	10 mol%
0/100	24 mol%	0 mol%	56 mol%	10 mol%	10 mol%

3.2 LNP CQA Characterization Studies

3.2.1 siRNA Encapsulation Efficiency

siRNA encapsulation and post-purification retention were quantified for all nanoparticle formulations at seven distinct timepoints (days 0, 1, 4, 7, 14, 21, and 28) using the Quant-iT™ RiboGreen™ RNA Assay (Invitrogen; ThermoFisher Scientific). At each timepoint, LNP samples were divided into two aliquots of equal volume. The first aliquot was lysed in the

presence of 1% (v/v) Triton X-100 and heparin (100 µg/mL) and incubated for 15 minutes at 37 °C to disrupt the lipid membrane and displace electrostatically associated siRNA, thereby releasing encapsulated cargo. The liberated siRNA was combined with RiboGreen reagent, and fluorescence was measured with emission collected at 525 nm. Fluorescence values from lysed samples were converted to siRNA content by interpolation from a standard curve generated using known siRNA concentrations prepared in an identical matrix (1% Triton X-100, 100 µg/mL heparin). Encapsulation efficiency (EE%) was calculated by:

$$\textbf{EE\%} = (\frac{\text{Encapsulated siRNA}}{\text{Total siRNA}}) * 100\% \tag{3.1}$$

To assess siRNA leakage and/or membrane stability, the RiboGreen assay was performed on the second aliquot of intact LNPs in the absence of Triton X-100 and heparin. Fluorescence from unlysed samples was measured to detect free (non-encapsulated or leaked) siRNA in the external aqueous phase, providing an index of formulation retention after purification. Percent leakage (% Leak) was calculated by:

$$\textbf{\% Leak} = (\frac{\text{Free siRNA}}{\text{Total siRNA}}) * 100\% \tag{3.2}$$

Six calibration standards were prepared to generate the concentration curve for both encapsulation efficiency and leakage measurements by spiking 0, 2.5, 5, 10, 20, and 40 pmol GAPDH siRNA from a 100 µM stock solution. The required total volume of RiboGreen working solution, for both EE% and % Leak assays, was calculated as:

$$\textbf{Total RiboGreen Working Volume } (\mu L) = 400 + [200 * (\#\text{ samples } + \#\text{ standards })] \tag{3.3}$$

The working RiboGreen solution was prepared by diluting the Ribogreen stock 1:200 in 1x TE buffer. The calculated volume yields sufficient reagent for both the encapsulation efficiency and the leakage assay.

3.2.2 Hydrodynamic Diameter and Homogeneity

The hydrodynamic diameter (Z-average; nm) and size distribution homogeneity (polydispersity index; PDI) of each LNP formulation were determined by dynamic light scattering (DLS) at each of the seven timepoints using a Zetasizer Nano ZS instrument (Malvern Instruments Ltd., Worcestershire, U.K.).

3.2.3 Zeta Potential

The membrane zeta potential (mV) of each LNP formulation was determined following dialysis in phosphate-buffered saline (PBS) by DLS using a Zetasizer Nano ZS instrument (Malvern Instruments Ltd., Worcestershire, U.K.). Measurements were conducted in triplicate using three independent replicates under identical experimental conditions.

3.3 In vitro Cellular Assays

3.3.1 Vascular Smooth Muscle Cell Cultures

Primary human aortic smooth muscle cells (HASMCs) were obtained in cryopreserved format from LifeLine Cell Technology LLC (Walkersville, MD, USA) and were originally isolated from a 17-year-old male donor. Cells were maintained at 37 °C in a humidified incubator equilibrated to 5% CO_2. HASMCs were cultured in VascuLife® Smooth Muscle Cell Growth Medium, consisting of VascuLife Basal Medium supplemented with the VascuLife smooth muscle cell supplement kit and gentamicin/amphotericin (LifeLine Cell Technology LLC, Federick, MD, U.S.A.).

3.3.2 Cellular Uptake Assay

For assessment of cellular uptake, LNPs were prepared as described above with incorporation of rhodamine-phosphatidylethanolamine (Rho-PE) at 1 mol% to enable fluorescence-based tracking. HASMCs were cultured to ∼80% confluence and serum-starved for 24 h in Dulbecco's Modified Eagle Medium (DMEM; ThermoFisher Scientific) to promote

a quiescent phenotype. Cells were then exposed for 24 h to rhodamine-labeled LNP formulations at a final concentration of 50 µM total lipid in VascuLife growth medium. Following treatment, cells were washed three times with 1x filtered PBS to remove non-internalized LNPs from culture.

Qualitative uptake was evaluated by fluorescence microscopy. Cells were fixed in formalin for 15 min prior to imaging, and fluorescence micrographs were acquired using an Olympus BX51 microscope equipped with an Olympus Q-Color Camera (Olympus Corporation, Shinjuku, Tokyo, Japan) at 100x magnification using a Texas Red filter set.

For quantitative uptake analysis, cells were detached by trypsinization, pelleted, and lysed in 1% (v/v) Triton X-100. Lysates were clarified by centrifugation at 12,000 rpm for 5 min to remove insoluble debris. Supernatants were plated in triplicate and fluorescence was measured by microplate fluorometry at an emission wavelength of 575 nm using a Modulus Microplate Multimode Reader (Promega Corporation, Madison, WI, USA). Uptake experiments were performed using n = 3 independent experimental replicates, with fluorescence values measured in triplicate wells after background subtraction.

3.3.3 Cytotoxicity Assay

LNP-associated cytotoxicity was evaluated in HASMCs. Cells were cultured to ∼60% confluence, serum-starved for 24 h, and then exposed for 24 h to LNP formulations at a final concentration of 50 µM total lipid in DMEM. Cell viability and cytotoxicity were quantified using the LIVE/DEAD™ Viability/Cytotoxicity Kit (Invitrogen; ThermoFisher Scientific) in accordance with the manufacturer's protocol. Briefly, culture medium was aspirated, cells were washed three times with PBS, and co-stained with calcein-AM and ethidium homodimer-1 for 15 min at 37 °C.

Fluorescence images were acquired using FITC (live) and Texas Red (dead) filter sets on an Olympus BX51 microscope at 100x magnification, with triplicate fields collected per condition for each channel. Live and dead cells were enumerated manually using Image-Pro Premier software (Media Cybernetics, Inc., Rockville, MD, USA). Percent cytotoxicity was

calculated for each field as:

$$\textbf{\% Cytotoxicity} = \left(\frac{\text{\# Dead}}{\text{\# Dead + \# Live}}\right) * 100\% \tag{3.4}$$

Cytotoxicity experiments were performed using n=3 independent experimental replicates, with triplicate microscopic fields analyzed for each formulation within each replicate.

3.4 Statistical Analysis

All data are presented as the mean ± standard error of the mean (SEM). Statistical comparisons were performed using Student's t-test and/or one-way analysis of variance (ANOVA), as appropriate for the experimental design. A probability P value < 0.05 was considered indicative of statistical significance.

Chapter 4

Results

4.1 Physicochemical Stability of Nanoparticles

4.1.1 Hydrodynamic Diameter/Size by DLS Z-Average

Across the 28-day stability assessment, hydrodynamic diameter remained within the nanoscale range for all DOPC/DOPE formulations, with all groups measuring below 100 nm at day 28. However, particle size exhibited a composition-dependent pattern, with DOPC-rich and intermediate formulations remaining smaller than DOPE-enriched formulations. The 100/0 DOPC/DOPE formulation increased from 56.61 nm at day 0 to 63.73 nm at day 28, corresponding to a net increase of 7.12 nm. The 75/25 formulation remained similar in size, increasing from 57.35 nm to 59.93 nm over the same period. The 50/50 formulation showed the smallest day-28 diameter, increasing modestly from 55.23 nm at day 0 to 57.47 nm at day 28.

In contrast, higher DOPE incorporation was associated with larger hydrodynamic diameters. The 25/75 formulation measured 70.16 nm at day 0 and 72.04 nm at day 28, while the 0/100 formulation increased from 66.94 nm to 75.47 nm. Longitudinally, the DOPC-rich and intermediate formulations showed narrower group-level ranges, including 56.05–63.73 nm for 100/0, 56.45–59.93 nm for 75/25, and 55.14–57.47 nm for 50/50. The DOPE-enriched groups exhibited larger overall ranges, particularly 25/75, which ranged from 64.70–126.92 nm, and 0/100, which ranged from 66.94–77.93 nm.

Table 4.1: Mean Hydrodynamic Diameter by Formulation

Group	Day 0	Day 28	Δ Days 0-28	Range
100/0	56.61	63.73	+7.12 nm	56.05-63.73
75/25	57.35	59.93	+2.58 nm	56.45-59.93
50/50	55.23	57.47	+2.24 nm	55.14-57.47
25/75	70.16	72.04	+1.88 nm	64.70-126.92
0/100	66.94	75.47	+8.53 nm	66.94-77.93

Units: nanometers (nm)

These formulation-dependent size trends are summarized in Table 4.1 and shown longitudinally in Figure 4.1. Although an elevated measurement contributed to the broader range observed in the 25/75 group, this value was not sustained across the full 28-day period. Therefore, it is reported descriptively as part of the observed size distribution rather than interpreted as definitive evidence of a formulation-specific aggregation event.

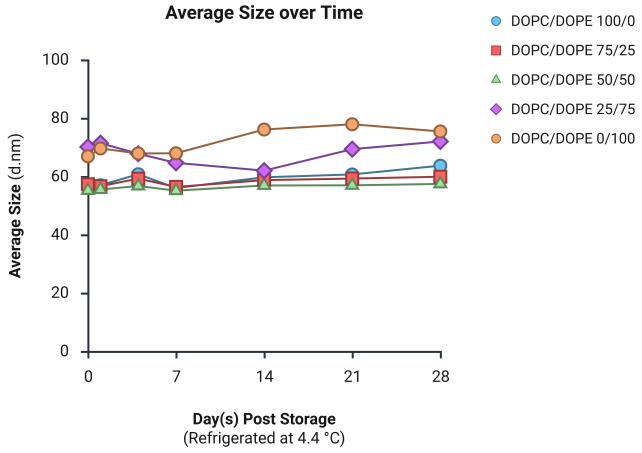

Figure 4.1: Measurements of Hydrodynamic Diameter.

Average particle size (d.nm) for each DOPC/DOPE formulation measured at 7 time-points over 28 days of storage at 4.4°C. Data are shown as group means over time with markers denoting each formulation.

4.1.2 Size Distribution Homogeneity by Polydispersity Index

Figure 4.2 demonstrates that, over the 28-day period, PDI values exhibited a monotonic increase with increasing DOPE molar fraction, with DOPE-enriched formulations consistently displaying higher central tendency and wider dispersion. The DOPC-only formulation

(100/0) yielded the lowest and most uniform PDI values across all timepoints (mean = 0.253; range = 0.2335-0.2945). The low-DOPE formulation (75/25) remained comparably low (mean = 0.272; range = 0.2472-0.3296), with the only observations exceeding 0.30 occurring at day 1 (0.3255 and 0.3296). Intermediate formulations demonstrated higher PDI values and increased variability, including 50/50 (mean = 0.356; range = 0.2990-0.4090) and 25/75 (mean = 0.412; range = 0.2611-0.4894). The DOPE-only formulation (0/100) was consistently the most heterogeneous across the dataset (mean = 0.516; range 0.4804-0.6084) and included the maximum observed PDI (0.6084).

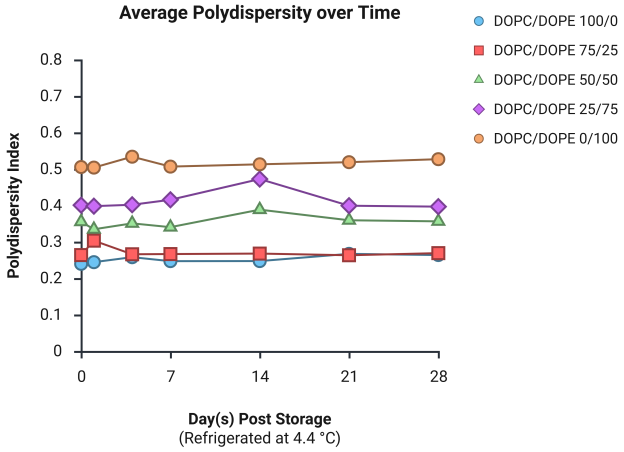

Figure 4.2: Measurements of Polydispersity Index.

Polydispersity index (PDI) for each DOPC/DOPE formulation (100/0, 75/25, 50/50, 25/75, 0/100) measured over 28 days of storage (days 0, 4, 7, 14, 21, 28) at 4.4°C. Data are shown as group means over time with markers denoting each formulation.

Using a commonly applied monodispersity threshold (PDI $\leq$ 0.30), all measurements for 100/0 satisfied this criterion, 19 of 21 measurements for 75/25, 6 of 21 in 50/50, and only 4 of 21 for 25/75. No measurements for 0/100 met the 0.30 PDI threshold at any timepoint.

4.2 siRNA Loading and Retention Performance

4.2.1 Encapsulation Efficiency (Triton/Heparin-lysed)

Encapsulation Efficiency (EE%) was quantified by RiboGreen fluorescence following chemical lysis (1% Triton X-100) with heparin displacement. EE% at day 0 was used as the primary measure of initial siRNA encapsulation for each formulation (n=3). Across all formulations day-0 EE% indicated high initial siRNA encapsulation, establishing successful loading at the time of preparation.

Table 4.2: Encapsulation Efficiency by Day

Group	100/0	75/25	50/50	25/75	0/100
Day 0	90.65±1.74%	102.21±1.48%	102.00±1.49%	103.36±0.89%	107.00±0.89%
Day 7	86.73±0.73%	96.40±1.49%	97.66±1.10%	97.13±3.53%	95.47±4.73%
Day 14	89.24±1.69%	102.40±1.41%	102.94±0.44%	100.84±0.86%	106.07±8.80%
Day 21	101.73±4.65%	115.23±2.38%	118.65±1.25%	122.39±0.85%	118.31±5.21%
Day 28	92.84±4.06%	100.52±3.22%	102.66±1.91%	105.70±0.46%	106.79±4.12%

To assess encapsulation stability during storage, EE% was re-measured at days 7, 14, 21, and 28 (n=3 per timepoint). For all formulations, EE% values at these timepoints were maintained relative to day 0, with no evidence of a time-dependent decline over the 28-day period. Measured EE% values occasionally exceeded 100%; consistent with assay restraints, these values were treated as non-physical readouts attributable to RiboGreen/standard-curve sensitivity rather than an increased siRNA content. Accordingly, the EE% dataset was interpreted as demonstrating stable siRNA encapsulation over time, using day 0 as the encapsulation benchmark and subsequent timepoints as stability comparisons alongside percent leakage.

4.2.2 siRNA Leakage/Externalized Cargo (Unlysed)

Percent leakage was assessed at each measured timepoint by RiboGreen fluorescence in the absence of Triton X-100. For all time points, the fluorescence signal for each sample remained below the fluorescence value of the 0 pmol siRNA standard, corresponding to a 0% to minimal leakage throughout the study interval. Thus, detectable siRNA release into

the external phase was minimal or not observed at any measured timepoint under the assay conditions and strengthens the high values for EE% previously provided.

4.2.3 Zeta Potential

Zeta-potential measurements indicated that all DOPC/DOPE formulations retained a net positive surface charge after dialysis. Mean zeta-potential values ranged from 8.27 mV to 13.85 mV across the formulation series. The DOPC-rich formulations exhibited the lowest average values, with 100/0 measuring 8.81 mV and 75/25 measuring 8.27 mV. Intermediate DOPE-containing formulations showed slightly higher mean values, with 50/50 measuring 10.03 mV and 25/75 measuring 10.56 mV. The DOPE-only formulation, 0/100, produced the highest mean zeta potential at 13.85 mV. These results are shown in Figure 4.3.

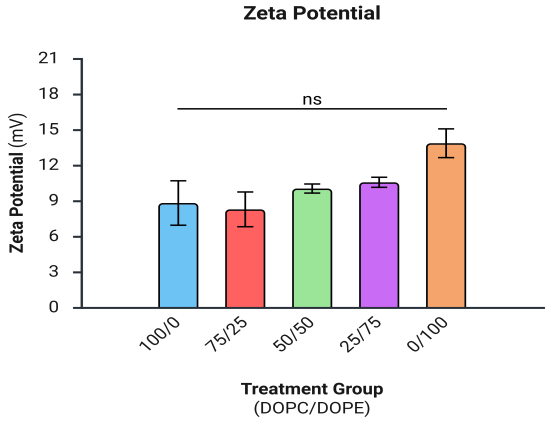

Figure 4.3: Measurements of Zeta Potential.

Zeta potential (mV) for each DOPC/DOPE formulation (100/0, 75/25, 50/50, 25/75, 0/100). Data are shown as mean zeta potential with associated variability across replicates for each formulation.

Although the zeta-potential values increased numerically with greater DOPE incorporation, this pattern was modest and should be interpreted descriptively. The difference between 100/0 and 75/25 did not follow a strictly monotonic pattern, and the overall dataset did not establish a statistically significant formulation-dependent shift in surface charge. Therefore,

these data indicate that helper lipid substitution may influence the electrostatic character of the nanoparticle surface, but they do not demonstrate a definitive or statistically supported charge transition across the DOPC/DOPE series.

Importantly, all formulations remained within a low-to-moderate positive zeta-potential range rather than developing a strongly cationic surface profile. Values near approximately +10 mV, and even the slightly higher value observed in the 0/100 formulation, are best interpreted as modest positive surface charge in the context of this formulation system. Thus, the zeta-potential results primarily show that all formulations retained weakly positive surface electrostatics after dialysis, with only a modest numerical increase in the DOPE-enriched groups.

4.3 Human Aortic Smooth Muscle Cell Assays

4.3.1 Cytotoxicity and Cellular Viability

For all DOPC/DOPE formulations, cytotoxicity in human aortic smooth muscle cells (HASMCs) remained low with all at or below 4.8%, with mean percent death increasing slightly as the DOPE fraction increased; however, this trend did not reach statistical significance by one-way ANOVA.

Baseline cell death (negative control) for this assay was 2.42 ± 0.14% (mean ± SD%; SEM = 0.080). Specific measurements of cytotoxicity by formulation are listed in Table 4.3.

Table 4.3: Percent Cytotoxicity by Formulation

Group	Mean ± SD%	SEM
100/0	3.32 ± 0.44%	0.254
75/25	3.74 ± 0.88%	0.509
50/50	4.31 ± 0.42%	0.240
25/75	4.64 ± 0.58%	0.334
0/100	4.78 ± 0.63%	0.365
N.C.	2.42 ± 0.14%	0.080

4.3.2 Quantitative Cellular Uptake

For the cellular uptake assay, active fluorescence units (AFU) were background-corrected by subtracting the negative control (N.C.) signal of 55.168 AFU from each replicate prior to averaging, shown in Table 4.4, and are reported as mean AFU ± SD. Uptake values were normalized to the lab-standard 100/0 DOPC/DOPE formulation, itself with a normalized AFU = 1.000, to enable direct comparison across the varying compositions.

Table 4.4: Mean Fluorescence from Cellular Uptake

Group	Adjusted AFU	Normalized AFU
100/0	97.357 ± 19.114	1.000
75/25	100.493 ± 15.817	1.032
50/50	182.770 ± 18.916	1.877
25/75	170.967 ± 14.124	1.756
0/100	302.627 ± 91.308	3.108
N.C.	55.168	N/A

Syntax: Mean AFU ± SD

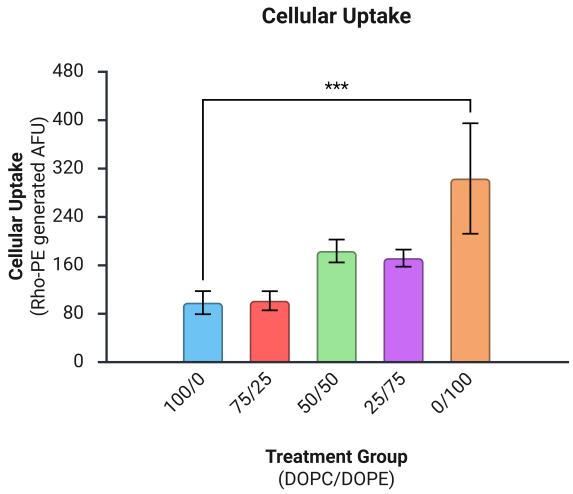

Figure 4.4: Fluorescent Cellular Uptake.

Input figure caption.

Quantitative fluorescence analysis demonstrated a composition-dependent increase in cellular uptake with increasing DOPE content 4.4. Relative to the 100/0 DOPC/DOPE formulation, the 75/25 formulation showed minimal change, whereas the 50/50 and 25/75

formulations showed intermediate increases. The 0/100 DOPE formulation produced the strongest uptake response, reaching approximately a 3.1-fold increase relative to 100/0 and representing the only statistically significant enhancement compared with the DOPC-only control.

Overall, normalized AFU increased with increasing DOPE fraction, with the strongest elevation observed at 0/100. All values represent three independent replicates (n=3). Normalized AFU values are reported relative to the 100/0 control.

Chapter 5

Discussion

5.1 Overview and Interpretation of Findings

The objective of this study was to determine how the progressive substitution of the helper phospholipid DOPE for DOPC within the patented R8-PLP lipid nanoparticle platform altered key formulation attributes relevant to siRNA delivery, including nanoparticle stability, encapsulation efficiency, cytotoxicity, and cellular uptake in human aortic smooth muscle cells. By keeping cholesterol, DSPE-PEG(2000), and STR-R8 constant while varying only the DOPC/DOPE ratio, the experimental design isolated helper lipid composition as the main independent variable affecting nanoparticle behavior.

Together, the results demonstrate that DOPC/DOPE substitution produced a clear composition-dependent tradeoff between colloidal stability and delivery-associated cellular performance. The DOPC-rich formulations remained smaller and more homogeneous throughout the 28-day storage interval, while the DOPE-enriched formulations exhibited larger hydrodynamic diameters, broader size distributions and increased surface charge. However, at the same time, increasing DOPE content was associated with maintained or slightly enhanced siRNA encapsulation and a marked increase in cellular uptake, while cytotoxicity remained low in all groups. These findings indicate that helper lipid composition did not simply affect one isolated property but instead shifted the overall physicochemical and biological profile of the nanoparticle platform in a coordinated manner.

Accordingly, the central implication of this study is that DOPE incorporation can improve delivery-relevant behavior, but excessive substitution reduces formulation uniformity. Thus, the most useful compositional range may not be the formulation that maximizes any single metric in isolation but rather the range that preserves sufficient stability while still improving uptake into target vascular cells. These findings are consistent with the original hypothesis that DOPC-rich systems would favor structural stability, while DOPE-rich systems would favor membrane activity and intracellular delivery.

5.2 Physicochemical Effects of Lipid Substitution

5.2.1 Hydrodynamic Diameter and Colloidal Stability

Hydrodynamic diameter is a primary critical quality attribute for lipid nanoparticles because particle size influences colloidal stability, cellular interaction, tissue access, and eventual in vivo disposition [14]. In the present 28-day storage study, all formulations remained within a nanoscale diameter range at the final timepoint, indicating that the R8-PLP platform retained overall particle integrity despite systematic variation in helper phospholipid composition. Importantly, all day-28 mean diameters remained below 100 nm, which is generally favorable for nucleic acid delivery applications and consistent with the formation of small lipid nanoparticle populations.

Within this overall stability profile, the size data revealed a clear formulation-dependent pattern. The 100/0, 75/25, and 50/50 formulations remained comparatively small and stable, with day-28 diameters of 63.73 nm, 59.93 nm, and 57.47 nm, respectively. In contrast, the 25/75 and 0/100 formulations exhibited larger diameters at both day 0 and day 28, suggesting that increasing DOPE content shifted the formulation toward larger particle populations. This trend is consistent with the expected biophysical effects of helper lipid substitution. DOPC contains a phosphatidylcholine headgroup that favors cylindrical molecular geometry and lamellar bilayer organization, whereas DOPE contains a smaller phosphatidylethanolamine headgroup that promotes negative curvature and non-lamellar

phase behavior. Thus, DOPC enrichment likely supported tighter lipid packing and smaller particle structure, while higher DOPE content favored more curvature-prone assemblies.

However, the size data should not be interpreted as evidence that DOPE substitution caused severe colloidal instability. The larger DOPE-rich formulations still remained within a generally acceptable nanoscale range at day 28. Instead, the diameter measurements suggest a moderate physical tradeoff: increasing DOPE content was associated with larger average particle size, while DOPC-rich and intermediate formulations better preserved smaller particle dimensions. This interpretation is strengthened when considered alongside the PDI data, where the major stability cost of DOPE substitution was reflected more clearly in formulation heterogeneity than in absolute particle diameter alone.

The elevated value observed in the 25/75 group should be interpreted cautiously. Because this increase was not sustained across the full storage period, it is more appropriately treated as an isolated measurement or technical fluctuation rather than as mechanistic evidence that the 25/75 formulation undergoes intermittent aggregation. Accordingly, the broader conclusion should be based on the overall longitudinal trend: DOPE-enriched formulations were larger and less size-consistent than DOPC-rich formulations, but the R8-PLP platform maintained nanoscale particle formation across the full DOPC/DOPE substitution series.

5.2.2 Polydispersity and Formulation Homogeneity

The PDI data strengthened the interpretation provided by the hydrodynamic diameter. Although size alone describes the central tendency, PDI provides a measure of how uniform or heterogeneous the nanoparticle population is. In the present study, PDI increased monotonically with increasing DOPE molar fraction, indicating that DOPE enrichment progressively broadened the size distribution and reduced the homogeneity of the formulation. The 100/0 formulation remained consistently monodisperse throughout the study period, and the 75/25 formulation remained near that range, except for isolated measurements above the 0.30 threshold. In contrast, the 50/50, 25/75, and 0/100 formulations showed substantially higher PDI values and greater variability.

This pattern is consistent with the biophysical properties of the helper lipids described in the background and rationale sections of the thesis. DOPC, although unsaturated, retains a phosphatidylcholine head-group that supports a relatively stable bilayer arrangement. DOPE, on the contrary, favors membrane curvature and fusogenicity, properties that are useful for destabilization events during intracellular trafficking, but can compromise the formulation of a narrowly distributed particle population. Thus, the observed rise in PDI with increasing DOPE content likely reflects a structural consequence of helper lipid-driven membrane packing differences rather than experimental noise alone.

Importantly, the PDI data indicate that the stability cost of DOPE substitution becomes much more pronounced beyond 50 mol % DOPE. Although 50/50 already showed diminished homogeneity compared to the DOPC-rich groups, the 25/75 and 0/100 formulations were clearly more heterogeneous. This suggests that moderate DOPE substitution may still be compatible with acceptable formulation quality, whereas high-DOPE conditions shift the system toward a less controlled colloidal state. Since formulation heterogeneity often affects the reproducibility, storage behavior, and interpretation of downstream biological assays, this finding argues against selecting the most DOPE-enriched system solely on the basis of uptake performance.

5.2.3 Encapsulation Efficiency and Cargo Retention

In contrast to size and PDI data, siRNA encapsulation efficiency remained strong throughout the entire formulation series. The day 0 encapsulation values were high for all groups, and subsequent measurements at later time points did not show evidence of time-dependent loss. In addition, leakage measurements remained minimal or below detection levels throughout the study interval. Taken together, these findings indicate that the R8-PLP platform retained robust cargo loading and retention performance regardless of the DOPC/DOPE ratio.

This result is especially meaningful because it suggests that helper lipid substitution did not compromise one of the most essential requirements for the function of RNA nanoparticles:

the successful incorporation of cargo and the stability over time. Since all formulations were prepared using the same 100:1 lipid:siRNA ratio, the same 10 mM $CaCl_2$-assisted condensation strategy, and the same STR-R8-containing PEGylated platform, the preserved encapsulation between groups implies that siRNA loading was dominated by the underlying condenser-enabled platform rather than by helper phospholipid identity alone.

The observation that several EE % values exceeded 100% does not materially weaken this conclusion, because these values were appropriately interpreted in Chapter 4 as assay-related non-physical readouts arising from RiboGreen or standard-curve sensitivity limitations rather than true increases in siRNA content. Furthermore, if the encapsulation efficiency were overstated, this unencapsulated siRNA would have been detected through the leakage assay over time. From this, no formulation showed poor loading and no formulation showed meaningful release during storage. Thus, helper lipid variation primarily affected physical stability and cellular interactions, while leaving cargo retention fundamentally intact.

5.2.4 Zeta Potential and Surface Electrostatics

Zeta-potential measurements demonstrated that all DOPC/DOPE formulations retained a modest net positive surface charge after dialysis, with mean values ranging from 8.27 mV to 13.85 mV. Numerically, the DOPC-rich formulations exhibited the lowest average zeta potentials, while the 0/100 formulation exhibited the highest average value. This pattern suggests that increasing DOPE content may alter the surface presentation or electrostatic environment of the nanoparticles. However, because the differences among groups were not statistically significant by one-way ANOVA, this trend should be interpreted as descriptive rather than inferential. The present data therefore do not establish that helper lipid substitution produced a definitive change in nanoparticle surface charge.

This distinction is important because DOPC and DOPE are both zwitterionic helper phospholipids; therefore, any observed shift in zeta potential is unlikely to reflect the introduction of a new formal cationic lipid species. Instead, the modest numerical increase in zeta potential may reflect changes in lipid packing, membrane curvature, or surface exposure of fixed formulation components such as STR-R8. Since cholesterol, DSPE-PEG(2000), and

STR-R8 were held constant across all groups, helper lipid composition may have altered how these components were organized or presented at the particle interface. However, the current data are insufficient to determine the precise structural basis of this effect.

The magnitude of the measured zeta potentials is also biologically relevant. Although all formulations were positively charged, the values were modest rather than strongly cationic. Measurements near approximately +10 mV generally indicate weak-to-moderate positive surface character, and even the highest mean value observed in the 0/100 formulation remained far below the highly cationic surface profiles typically associated with pronounced membrane disruption or nonspecific cytotoxicity. This interpretation is consistent with the cytotoxicity results, where all formulations produced low levels of cell death under the 24-hour exposure conditions tested.

Accordingly, zeta potential should not be used as the primary mechanistic explanation for the enhanced cellular uptake observed in DOPE-enriched formulations. Although a more positive surface charge could theoretically increase electrostatic interaction with negatively charged cell membranes, the lack of statistical significance in the zeta-potential dataset prevents a causal interpretation. The uptake enhancement observed in the 0/100 formulation is therefore more plausibly interpreted as the combined result of DOPE-associated membrane curvature, fusogenicity, and altered particle-cell interactions, rather than as a charge-driven effect alone. Future studies with larger replicate numbers, serum-containing electrokinetic measurements, and direct assays of endosomal escape would be required to determine whether surface charge contributes meaningfully to functional delivery.

5.3 Formulation Performance in vitro

5.3.1 Cytotoxicity and Cellular Viability

For any candidate anti-restenotic nanoparticle platform, low cytotoxicity in vascular smooth muscle cells is critical. In the present study, all formulations produced low levels of cell death, with mean cytotoxicity values remaining below 5% % in the entire DOPC/DOPE range. Although a gradual increase in percent death was observed as DOPE content

increased, these differences remained small in magnitude, and the overall assay profile suggests that none of the helper lipid ratios tested produced overt toxicity under the 24-hour exposure conditions used here.

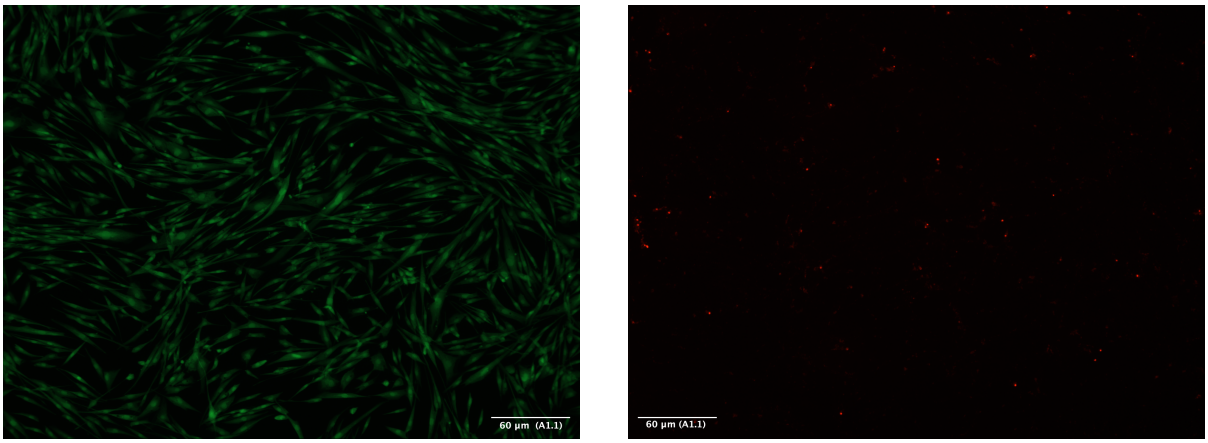

(a) 100/0 LIVE **(b)** 100/0 DEAD

Figure 5.1: 100/0 Formulation LIVE/DEAD Cytotoxicity

This finding is important for two main reasons. First, it indicates that the observed increases in uptake for higher-DOPE formulations were not accompanied by a proportionate increase in acute cytotoxicity, which strengthens the interpretation that greater fluorescence reflected improved cell-associated delivery rather than nonspecific membrane damage alone. Second, it supports continued use of the R8-PLP backbone for vascular applications, since the fixed inclusion of STR-R8, cholesterol, and DSPE-PEG(2000) did not generate strong toxicity in primary HASMCs even when the helper lipid composition was altered.

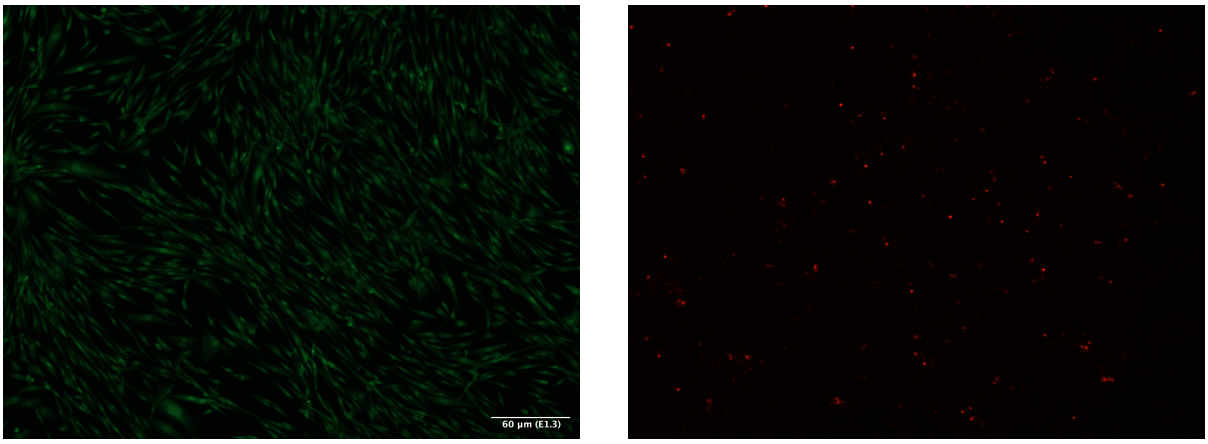

(a) 0/100 LIVE **(b)** 0/100 DEAD

Figure 5.2: 0/100 Formulation LIVE/DEAD Cytotoxicity

At the same time, the slight upward trend in cell death with increasing DOPE should not be ignored. It may reflect that formulations with more fusogenic or more positively charged atoms interact more aggressively with cellular membranes. Although this did not produce prohibitive toxicity in the present assay window, it suggests that future work should include broader dose-response and time-course analyses to determine whether the same trend becomes more pronounced under longer exposure or at higher lipid concentrations.

5.3.2 Quantitative Cellular Uptake

Among all endpoints measured in this study, cellular uptake showed the clearest functional benefit of DOPE incorporation. After background correction and normalization to the 100/0 control, uptake remained essentially unchanged in the 75/25 formulation, but increased substantially in the 50/50, 25/75, and 0/100 groups, with the largest effect observed in the DOPE-only formulation. Thus, unlike the stability metrics, which progressively worsened with increasing DOPE, uptake improved progressively and reached its maximum under the most DOPE-enriched condition.

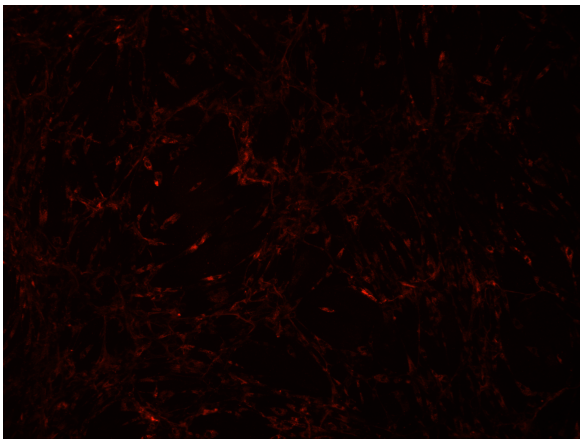

(a) 100/0 Uptake

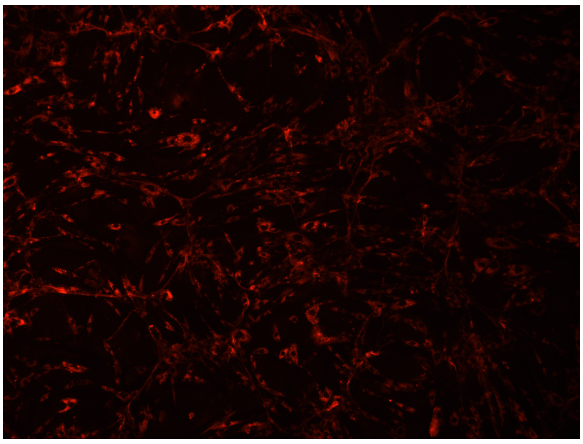

(b) 75/25 Uptake

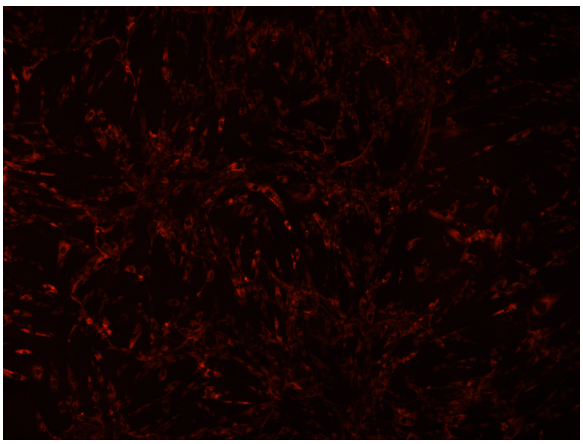

(c) 50/50 Uptake

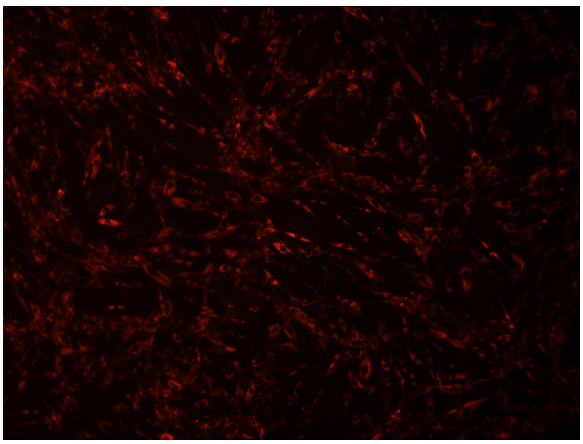

(d) 25/75 Uptake

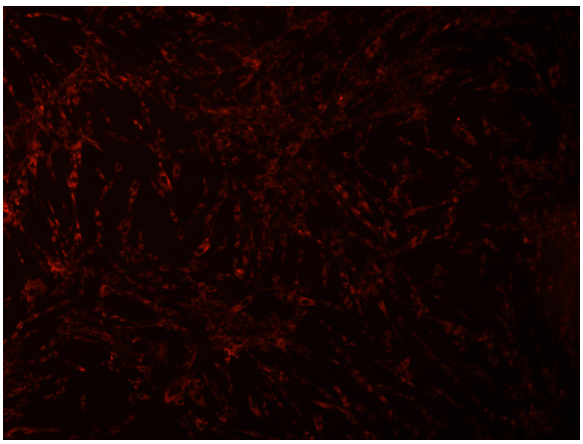

(e) 0/100 Uptake

(f) N.C. Uptake

Figure 5.3: Fluorescent Cellular Uptake

This result is well aligned with the mechanistic rationale that motivated the substitution of helper lipids in the first place. DOPE is widely regarded as a fusogenic phospholipid whose cone-shaped geometry promotes curvature stress and non-lamellar phase behavior relevant to membrane destabilization and intracellular delivery. Within the present platform, these properties may have increased interaction with HASMC membranes, improved internalization, or enhanced intracellular trafficking of fluorescently labeled nanoparticles. The rise in zeta potential observed in parallel with a rise in the DOPE content may also have contributed by increasing the electrostatic interaction with negatively charged cell surfaces.

However, the uptake data should be interpreted carefully. The present assay quantified rhodamine-associated cellular fluorescence rather than direct measurement of functional siRNA silencing. Therefore, the observed increase most directly indicates greater nanoparticle association and/or internalization, not necessarily improving the cytosolic delivery of intact siRNA or stronger RNAi activity. The distinction is important because fluorescence-based uptake can overestimate meaningful therapeutic delivery if particles are internalized but remain trapped in endosomal compartments. Consequently, the uptake advantage of high-DOPE formulations is promising but not yet sufficient to establish superior therapeutic performance without follow-up knockdown studies.

Chapter 6

Conclusions and Future Directions

6.1 Integrated Interpretation and Tradeoffs

When the physicochemical and cellular datasets are considered together, a coherent pattern emerges. Increasing DOPE content improved the apparent biological delivery, as reflected by greater uptake and slightly more positive surface charge, but this occurred along with increasing particle size and, more importantly, increasing heterogeneity. Meanwhile, encapsulation remained strong and leakage was minimal in all groups, indicating that the loading of the cargo itself was not the limiting factor in any formulation. Thus, the principal tradeoff introduced by the DOPE substitution was not between loading and uptake, but between colloidal uniformity and delivery-associated cellular interaction.

This integrated interpretation suggests that the optimal formulation window likely lies in the intermediate DOPE range rather than at either compositional extreme. The 100/0 formulation showed the greatest uniformity and stability, but comparatively modest cellular uptake. The 0/100 formulation showed the strongest uptake, but also the greatest heterogeneity and the highest zeta potential. Intermediate formulations, particularly 50/50 and to some extent 25/75, appear to preserve much of the uptake benefit of DOPE while avoiding the most extreme loss of colloidal control. From a formulation-development perspective, this middle range may represent the most rational starting point for continued

optimization.

This conclusion is consistent with the broader logic of nanoparticle design in which the best therapeutic candidate is rarely one that maximizes a single physicochemical or cellular readout. Rather, effective systems must balance manufacturability, storage stability, safety, cargo retention, and biologic function. In the present study, intermediate DOPE substitution appears to offer the strongest balance between those competing requirements.

6.2 Study Limitations and Future Directions

Several limitations of the present work should be acknowledged. The study evaluated uptake and cytotoxicity in vitro using primary HASMCs but did not directly measure gene silencing, protein suppression, or other downstream RNAi outcomes. As a result, the functional consequences of the increased uptake observed in DOPE-enriched formulations remain inferential rather than demonstrated. Second, while three independent replicates are sufficient to identify major trends, larger numbers of replicates would improve confidence in subtle differences between intermediate formulations. Lastly, zeta potential was measured after dialysis in PBS, which is appropriate for comparative characterization, but does not fully capture how surface electrostatics and corona formation may change in serum-containing biological environments.

In addition, the storage study focused on size, PDI, and cargo retention over 28 days, but did not include higher-resolution structural methods such as TEM or cryo-EM. Therefore, the present interpretation of DOPE-driven structural changes is necessarily indirect and is based on established lipid biophysics together with DLS-derived outputs. Future work should also determine whether the uptake advantage of DOPE-enriched groups translates into improved endosomal escape and functional silencing of disease-relevant targets in vascular smooth muscle cells.

Consequently, the next logical step is the direct evaluation of the RNAi performance, such as the removal of GAPDH by RT-qPCR or protein-level analysis, in the most promising formulation window. Such experiments would determine whether the increase in fluorescence observed in the uptake assay corresponds to therapeutically meaningful intracellular delivery. Additional studies examining serum stability, dose dependence, and long-term compatibility would also strengthen translational interpretation.

6.3 Overall Conclusion

In summary, this project has demonstrated that the helper phospholipid composition exerts a strong and coordinated influence on the behavior of the patented R8-PLP siRNA nanoparticle platform. DOPC-rich formulations favored smaller and more homogeneous nanoparticles, whereas DOPE enrichment increased positive surface charge and substantially improved HASMC uptake. The encapsulation efficiency remained high and leakage remained minimal across all formulations, indicating that the base platform robustly retained the siRNA cargo independently of the helper lipid ratio. Similarly, cytotoxicity remained low in all formulation series.

The most important conclusion is that DOPE incorporation improved the cellular behavior associated with delivery, but excessive substitution reduced physicochemical uniformity. Therefore, the data support an intermediate compositional window, rather than either extreme, as the most promising direction for continued development. In practical terms, formulations around 50/50 DOPC/DOPE appear to be best positioned to balance colloidal stability with improved delivery potential in human aortic smooth muscle cells. The balance is especially relevant for anti-restenotic RNAi applications, where both nanoparticle stability and effective cellular delivery are required for successful therapeutic performance.

Bibliography

[1] Adams, D., Gonzalez-Duarte, A., O'Riordan, W. D., Yang, C. C., Ueda, M., Kristen, A. V., Tournev, I., Schmidt, H. H., Coelho, T., Berk, J. L., Lin, K. P., Vita, G., Attarian, S., Plante-Bordeneuve, V., Mezei, M. M., Campistol, J. M., Buades, J., Brannagan, T. H., r., Kim, B. J., Oh, J., Parman, Y., Sekijima, Y., Hawkins, P. N., Solomon, S. D., Polydefkis, M., Dyck, P. J., Gandhi, P. J., Goyal, S., Chen, J., Strahs, A. L., Nochur, S. V., Sweetser, M. T., Garg, P. P., Vaishnaw, A. K., Gollob, J. A., and Suhr, O. B. (2018). Patisiran, an rnai therapeutic, for hereditary transthyretin amyloidosis. *N Engl J Med*, 379(1):11–21. 3

[2] Agrawal, N., Dasaradhi, P. V., Mohmmed, A., Malhotra, P., Bhatnagar, R. K., and Mukherjee, S. K. (2003). Rna interference: biology, mechanism, and applications. *Microbiol Mol Biol Rev*, 67(4):657–85. 15

[3] Bartel, D. P. (2004). Micrornas: genomics, biogenesis, mechanism, and function. *Cell*, 116(2):281–97. 16

[4] Bartel, D. P. (2009). Micrornas: target recognition and regulatory functions. *Cell*, 136(2):215–33. 16

[5] Cedervall, T., Lynch, I., Lindman, S., Berggard, T., Thulin, E., Nilsson, H., Dawson, K. A., and Linse, S. (2007). Understanding the nanoparticle-protein corona using methods to quantify exchange rates and affinities of proteins for nanoparticles. *Proc Natl Acad Sci U S A*, 104(7):2050–5. 7

[6] Chan, W. C. and Nie, S. (1998). Quantum dot bioconjugates for ultrasensitive nonisotopic detection. *Science*, 281(5385):2016–8. 9

[7] Chi, S. W., Hannon, G. J., and Darnell, R. B. (2012). An alternative mode of microrna target recognition. *Nat Struct Mol Biol*, 19(3):321–7. 16

[8] Crooke, S. T., Baker, B. F., Crooke, R. M., and Liang, X. H. (2021). Antisense technology: an overview and prospectus. *Nat Rev Drug Discov*, 20(6):427–453. 15

[9] Egli, M. and Manoharan, M. (2023). Chemistry, structure and function of approved oligonucleotide therapeutics. *Nucleic Acids Res*, 51(6):2529–2573. 17

[10] Elbashir, S. M., Harborth, J., Lendeckel, W., Yalcin, A., Weber, K., and Tuschl, T. (2001). Duplexes of 21-nucleotide rnas mediate rna interference in cultured mammalian cells. *Nature*, 411(6836):494–8. 13

[11] Finkel, R. S., Mercuri, E., Darras, B. T., Connolly, A. M., Kuntz, N. L., Kirschner, J., Chiriboga, C. A., Saito, K., Servais, L., Tizzano, E., Topaloglu, H., Tulinius, M., Montes, J., Glanzman, A. M., Bishop, K., Zhong, Z. J., Gheuens, S., Bennett, C. F., Schneider, E., Farwell, W., De Vivo, D. C., and Group, E. S. (2017). Nusinersen versus sham control in infantile-onset spinal muscular atrophy. *N Engl J Med*, 377(18):1723–1732. 17

[12] Fire, A., Xu, S., Montgomery, M. K., Kostas, S. A., Driver, S. E., and Mello, C. C. (1998). Potent and specific genetic interference by double-stranded rna in caenorhabditis elegans. *Nature*, 391(6669):806–11. 12

[13] Fisher, R. K., Mountain, D. J. H., and Grandas, O. H. (2025). Methods of making neutral liposomes containing biologically active agents. 22

[14] Fisher, R. K., Mountain, D. J. H., and Grandas, O. H. (2026). Neutral liposomes containing biologically active agents. 22, 23, 39

[15] Geary, R. S., Norris, D., Yu, R., and Bennett, C. F. (2015). Pharmacokinetics, biodistribution and cell uptake of antisense oligonucleotides. *Adv Drug Deliv Rev*, 87:46–51. 17, 18

[16] Giner-Casares, J. J., Henriksen-Lacey, M., Coronado-Puchau, M., and Liz-Marzán, L. M. (2016). Inorganic nanoparticles for biomedicine: where materials scientists meet medical research. *Materials Today*, 19(1):19–28. 9

[17] Guerrero, E. D., Vaidya, A., Santelli, J., Tian, Z., Pazzi, G. A., and Siegwart, D. J. (2026). Investigating the functional contributions of phospholipids in selective organ targeting lipid nanoparticles. *Biomaterials*, 326:123671. 20

[18] Guo, H., Ingolia, N. T., Weissman, J. S., and Bartel, D. P. (2010). Mammalian micrornas predominantly act to decrease target mrna levels. *Nature*, 466(7308):835–40. 16

[19] Hald Albertsen, C., Kulkarni, J. A., Witzigmann, D., Lind, M., Petersson, K., and Simonsen, J. B. (2022). The role of lipid components in lipid nanoparticles for vaccines and gene therapy. *Adv Drug Deliv Rev*, 188:114416. 19, 20

[20] Hammond, S. M., Bernstein, E., Beach, D., and Hannon, G. J. (2000). An rna-directed nuclease mediates post-transcriptional gene silencing in drosophila cells. *Nature*, 404(6775):293–6. 12, 13

[21] Han, J., Lee, Y., Yeom, K. H., Kim, Y. K., Jin, H., and Kim, V. N. (2004). The drosha-dgcr8 complex in primary microrna processing. *Genes Dev*, 18(24):3016–27. 16

[22] Huang, X., Jain, P. K., El-Sayed, I. H., and El-Sayed, M. A. (2007). Gold nanoparticles: interesting optical properties and recent applications in cancer diagnostics and therapy. *Nanomedicine (Lond)*, 2(5):681–93. 9

[23] Jung, H. N., Lee, S. Y., Lee, S., Youn, H., and Im, H. J. (2022). Lipid nanoparticles for delivery of rna therapeutics: Current status and the role of in vivo imaging. *Theranostics*, 12(17):7509–7531. 19, 21

[24] Kim, D., Kim, J., Park, Y. I., Lee, N., and Hyeon, T. (2018). Recent development of inorganic nanoparticles for biomedical imaging. *ACS Cent Sci*, 4(3):324–336. 9

[25] Kuchler, A., Yoshimoto, M., Luginbuhl, S., Mavelli, F., and Walde, P. (2016). Enzymatic reactions in confined environments. *Nat Nanotechnol*, 11(5):409–20. Kuchler, Andreas Yoshimoto, Makoto Luginbuhl, Sandra Mavelli, Fabio Walde, Peter eng Research Support, Non-U.S. Gov't Review England 2016/05/06 Nat Nanotechnol. 2016 May 5;11(5):409-20. doi: 10.1038/nnano.2016.54. 11

[26] Lee, R. C., Feinbaum, R. L., and Ambros, V. (1993). The c. elegans heterochronic gene lin-4 encodes small rnas with antisense complementarity to lin-14. *Cell*, 75(5):843–54. 16

[27] Lee, Y., Ahn, C., Han, J., Choi, H., Kim, J., Yim, J., Lee, J., Provost, P., Radmark, O., Kim, S., and Kim, V. N. (2003). The nuclear rnase iii drosha initiates microrna processing. *Nature*, 425(6956):415–9. 16

[28] Lee, Y., Kim, M., Han, J., Yeom, K. H., Lee, S., Baek, S. H., and Kim, V. N. (2004). Microrna genes are transcribed by rna polymerase ii. *EMBO J*, 23(20):4051–60. 16

[29] Levin, A. A. (2019). Treating disease at the rna level with oligonucleotides. *N Engl J Med*, 380(1):57–70. 17, 18

[30] Lundqvist, M., Stigler, J., Elia, G., Lynch, I., Cedervall, T., and Dawson, K. A. (2008). Nanoparticle size and surface properties determine the protein corona with possible implications for biological impacts. *Proc Natl Acad Sci U S A*, 105(38):14265–70. 12

[31] Maeda, H., Wu, J., Sawa, T., Matsumura, Y., and Hori, K. (2000). Tumor vascular permeability and the epr effect in macromolecular therapeutics: a review. *J Control Release*, 65(1-2):271–84. 7

[32] Monopoli, M. P., Aberg, C., Salvati, A., and Dawson, K. A. (2012). Biomolecular coronas provide the biological identity of nanosized materials. *Nat Nanotechnol*, 7(12):779–86. 12

[33] Mullard, A. (2018). Low-cost non-profit drug repurposing. *Nat Rev Drug Discov*, 18(1):7. Mullard, Asher eng England 2018/12/29 Nat Rev Drug Discov. 2018 Dec 28;18(1):7. doi: 10.1038/nrd.2018.228. 11

[34] Navid Talemi, M., Ramezani Farani, M., Alipour Eskandani, N., Mirzaee, D., Alipourfard, I., and Huh, Y. S. (2026). Programmable lipid nanoparticles for rna therapeutics: Design principles and clinical translation. *Mater Today Bio*, 37:102774. 18

[35] Paddison, P. J., Caudy, A. A., Bernstein, E., Hannon, G. J., and Conklin, D. S. (2002). Short hairpin rnas (shrnas) induce sequence-specific silencing in mammalian cells. *Genes Dev*, 16(8):948–58. 15

[36] Pardi, N., Hogan, J. M., Porter, W. F., and Weissman, D. (2018). mrna vaccines — a new era in vaccinology. *Nature Reviews Drug Discovery*, 17(4):261–279. 10

[37] Reinhart, B. J., Slack, F. J., Basson, M., Pasquinelli, A. E., Bettinger, J. C., Rougvie, A. E., Horvitz, H. R., and Ruvkun, G. (2000). The 21-nucleotide let-7 rna regulates developmental timing in caenorhabditis elegans. *Nature*, 403(6772):901–6. 16

[38] Roberts, T. C., Langer, R., and Wood, M. J. A. (2020). Advances in oligonucleotide drug delivery. *Nat Rev Drug Discov*, 19(10):673–694. 17

[39] Summers, H. (2011). Bionanoscience: Nanoparticles in the life of a cell. *Nat Nanotechnol*, 7(1):9–10. 7

[40] Suna, G., Wojakowski, W., Lynch, M., Barallobre-Barreiro, J., Yin, X., Mayr, U., Baig, F., Lu, R., Fava, M., Hayward, R., Molenaar, C., White, S. J., Roleder, T., Milewski, K. P., Gasior, P., Buszman, P. P., Buszman, P., Jahangiri, M., Shanahan, C. M., Hill, J., and Mayr, M. (2018). Extracellular matrix proteomics reveals interplay of aggrecan and aggrecanases in vascular remodeling of stented coronary arteries. *Circulation*, 137(2):166–183. 1

[41] Syama, K., Jakubek, Z. J., Chen, S., Zaifman, J., Tam, Y. Y. C., and Zou, S. (2022). Development of lipid nanoparticles and liposomes reference materials (ii): cytotoxic profiles. *Sci Rep*, 12(1):18071. 13, 18

[42] Vallet-Regi, M., Balas, F., and Arcos, D. (2007). Mesoporous materials for drug delivery. *Angew Chem Int Ed Engl*, 46(40):7548–58. 9

[43] Vervaeke, P., Borgos, S. E., Sanders, N. N., and Combes, F. (2022). Regulatory guidelines and preclinical tools to study the biodistribution of rna therapeutics. *Adv Drug Deliv Rev*, 184:114236. 14

[44] Wilensky, R. L., March, K. L., Gradus-Pizlo, I., Sandusky, G., Fineberg, N., and Hathaway, D. R. (1995). Vascular injury, repair, and restenosis after percutaneous transluminal angioplasty in the atherosclerotic rabbit. *Circulation*, 92(10):2995–3005. 1

[45] Yi, R., Qin, Y., Macara, I. G., and Cullen, B. R. (2003). Exportin-5 mediates the nuclear export of pre-micrornas and short hairpin rnas. *Genes Dev*, 17(24):3011–6. 15

[46] Yoshida, T., Naito, Y., Yasuhara, H., Sasaki, K., Kawaji, H., Kawai, J., Naito, M., Okuda, H., Obika, S., and Inoue, T. (2019). Evaluation of off-target effects of gapmer antisense oligonucleotides using human cells. *Genes Cells*, 24(12):827–835. 17, 18

Appendix

A Lipid Nanoparticle Formulation Sheets

The following tables outline the specific volumes of each constituent combined during the synthesis of each formulation of lipid nanoparticles:

Table A.1: 100/0 DOPC/DOPE Formulation Sheet

Lipid	**Mol. Percent** (mol%)	**Mol. Mass** (g/mol)	**Stock Conc.** (mM)	**Vol. Needed** (μL)
Cholesterol	24	386.654	6.466	38.39
DOPC	56	786.113	12.721	45.53
DOPE	0	744.034	13.440	0.00
DSPE-PEG	10	2805.497	3.564	29.02
STR-R8	10	1533.01	3.262	31.71

The 100/0 DOPC/DOPE formulation is the laboratory 'standard' that is most consistent with the base R8-PLP formulation.

Table A.2: 75/25 DOPC/DOPE Formulation Sheet

Lipid	**Mol. Percent** (mol%)	**Mol. Mass** (g/mol)	**Stock Conc.** (mM)	**Vol. Needed** (μL)
Cholesterol	24	386.654	6.466	38.63
DOPC	42	786.113	12.721	34.36
DOPE	14	744.034	13.440	10.84
DSPE-PEG	10	2805.497	3.564	29.19
STR-R8	10	1533.01	3.262	31.91

Table A.3: 50/50 DOPC/DOPE Formulation Sheet

Lipid	**Mol. Percent** (mol%)	**Mol. Mass** (g/mol)	**Stock Conc.** (mM)	**Vol. Needed** (μL)
Cholesterol	24	386.654	6.466	38.86
DOPC	28	786.113	12.721	23.05
DOPE	28	744.034	13.440	21.81
DSPE-PEG	10	2805.497	3.564	29.38
STR-R8	10	1533.01	3.262	31.10

Table A.4: 25/75 DOPC/DOPE Formulation Sheet

Lipid	**Mol. Percent** (mol%)	**Mol. Mass** (g/mol)	**Stock Conc.** (mM)	**Vol. Needed** (μL)
Cholesterol	24	386.654	6.466	39.11
DOPC	14	786.113	12.721	11.59
DOPE	42	744.034	13.440	32.92
DSPE-PEG	10	2805.497	3.564	29.56
STR-R8	10	1533.01	3.262	32.30

Table A.5: 0/100 DOPC/DOPE Formulation Sheet

Lipid	**Mol. Percent** (mol%)	**Mol. Mass** (g/mol)	**Stock Conc.** (mM)	**Vol. Needed** (μL)
Cholesterol	24	386.654	6.466	39.35
DOPC	0	786.113	12.721	0.00
DOPE	56	744.034	13.440	44.17
DSPE-PEG	10	2805.497	3.564	29.74
STR-R8	10	1533.01	3.262	32.50

Special Terms and Abbreviations

Ago2 Argonaute2. 13

ASO Antisense Oligonucleotide. 15–17

CPP Cell-penetrating peptide. 10, 22, 23

CQA Critical Quality Attributes. 4

cryo-EM Cryogenic Electron Microscopy. 8

DLS Dynamic Light Scattering. 7

DOPC 1,2-dioleoyl-sn-glycero-3-phosphatidylcholine. 3, 19

DOPE 1,2-dioleoyl-sn-glycero-3-phosphatidylethanolamine. 3, 20

DSPC 1,2-distearoyl-sn-glycero-3-phosphocholine). 19

dsRNA Double-stranded RNA. 12, 13

EPR Enhanced Permeability and Retention Effect. 7

EV Extracellular vesicle. 11

INP Inorganic nanoparticle. 8

LNP Lipid Nanoparticle. 2, 12

mRNA Messenger RNA. 2, 17

NP Nanoparticle. 10

NTA Nanoparticle Tracking Analysis. 7

PDI Polydispersity Index. 4, 23

PLP Primary Lipid Platform. 22, 23

RdRPs RNA-dependent RNA polymerases. 14

RISC RNA-induced silencing complex. 2, 13

RNAi RNA Interference. 2, 12

shRNA Short Hairpin RNA. 14

siRNA Small Interfering RNA. 2, 13, 14, 23

STR-R8 Stearylated Octaarginine. 22, 23

TEM Transmission Electron Microscopy. 8

VSMC Vascular Smooth Muscle Cells. 1

Vita

Graham Cole Goforth is a candidate for the Bachelor of Science in Honors Biochemistry and Cellular/Molecular Biology at the University of Tennessee, Knoxville, with graduation expected in May 2026. His honors thesis, conducted in the Vascular Research Laboratory at the University of Tennessee Graduate School of Medicine under the direction of Dr. Deidra Mountain, examines the optimization of lipid nanoparticles for stability, cytotoxicity, and cellular uptake through variation of phospholipid composition. His undergraduate research has included lipid nanoparticle synthesis, organic chemical synthesis, microplastics bioaccumulation, and more. He has served as an undergraduate teaching assistant in biology and biochemistry laboratory courses. Following his graduation, he plans to begin doctoral study in Biological Sciences at Vanderbilt University in August 2026.